STUDY OF A SLENDER MASONRY WALL TESTED IN AN INNOVATIVE DEVICE

by

Rafael De Jesus Gonzalez Mariscal

A thesis submitted in partial fulfillment of the requirements for the degree of

Master of Science

in

STRUCTURAL ENGINEERING

Department of Civil and Environmental Engineering

University of Alberta

ABSTRACT

Slender masonry walls are often found in school gymnasiums, warehouses and other low-rise buildings. According to current North American masonry design standards, a slender wall is defined to have a height-to-thickness ratio of 30 or greater. These walls must satisfy several stringent requirements as they are more susceptible to second-order effects, and it is believed that they present early instability issues. However, only a few experimental tests have been conducted to understand the true nature of slender masonry walls. Moreover, recent studies show that provisions in the standards are overly conservative and lead to non-economical designs. This study is the starting point of a research campaign that aims to address the need for more experimental tests on full-scale slender masonry walls.

A numerical model using the software OpenSEES proved to closely predict the response of slender masonry walls subject to a combination of vertical and out-of-plane loads. The model was used to perform a parametric study to understand the behaviour of these walls under a variety of conditions and propose a promising solution to increase the stiffness of concrete masonry walls. Results of the parametric study also showed that walls were unstable shortly after the reinforcement yielded, suggesting that the requirement of a ductile failure mode in the standards should be re-evaluated. Then, an 8.75 m tall concrete masonry wall was built on a specially designed test setup. The wall was tested under a combination of vertical and cyclic out-of-plane loads, and under pin-end conditions. The importance of having a displacement limit in the standards was evident after pushing the wall to a midspan displacement equal to the serviceability limit of $h/180$ (48 mm) required by S304-14. After unloading, the residual displacement at midspan was already equal to 8 mm, indicating some damage and loss of out-of-plane stiffness. After a few

cycles and when the sensors had indicated yielding of the vertical reinforcement, the test was stopped.

Sensor readings showed that the maximum moment was not located at midspan but higher. This suggests that different loading conditions may have been present in the test, such as a differential pressure applied by the airbag or some friction present on the pinned supports. It was also found that the neutral axis was within the face shell of the concrete block from the early stages of loading. This means that the grouted portion of the cross-section contributed very little to the wall response, probably only before cracking. It also shows that the ungrouted properties of the masonry are highly relevant for the response of these walls.

The behaviour of the wall after cracking was mainly affected by the area and location of vertical reinforcement. If the vertical bars were defined as centrally located in the cross-section of the numerical model, the wall stiffness was underestimated when compared to test results. This may be explained if steel bars were deviated from their original position farther from the compressive face of the wall during the grouting process, resulting in a larger post-cracking stiffness and a larger yielding load.

PREFACE

Chapter 3 of this thesis has been published as R. Gonzalez, A. Alonso, C. Cruz, and D. Tomlinson, "Numerical Study of the Response of Reinforced Slender Masonry Walls with Various Reinforcement Arrangements" in the proceedings of the 14th Canadian Masonry Symposium in Montreal, Canada. I was responsible for the model development and analysis as well as the manuscript composition. A. Alonso and C. Cruz were involved with concept formation and manuscript composition. D. Tomlinson was the supervisory author and was involved with concept formation and manuscript composition.

Some of the work conducted for this thesis forms part of a research collaboration led by Professor Carlos Cruz-Noguez and Professor Douglas Tomlinson at the University of Alberta. The design of the test setup presented in chapter 4 and the experimental test referred to in chapter 4 were performed with the assistance of Alan Alonso and Mahmoud Elsayed. The literature review in chapter 2, the data analysis in chapter 4 and the conclusions presented in chapter 5 are my original work.

DEDICATION

This thesis is dedicated to my wife, Gabriela, and my daughter, Abril. You have been a constant source of support and encouragement during the development of this work. Thank you for your understanding and for all the sacrifices you have endured for me to pursue this dream.

And to my loving parents, Carlos and Leticia. Thank you for the unconditional love and kindness. I would have never enjoyed so many opportunities without your help.

ACKNOWLEDGEMENTS

I would like to thank my supervisor, Dr. Douglas Tomlinson, for his support and guidance during this research project. I would like to also thank Dr. Carlos Cruz-Noguez for his advice and continuous encouragement. I would not have been able to complete this journey without them. I am eternally grateful to both for taking a chance on a foreign student with no more than a desire to learn.

To my colleagues and friends, Alan Alonso and Mahmoud Elsayed, thank you for sharing your time and knowledge to make this work possible. I feel extremely fortunate to have worked with such talented engineers in the development of the experimental component of this work.

A special thanks to the University of Alberta lab technicians Greg Miller and Cameron West. My research would not have been possible without their help.

Funding for this research has been provided by the Masonry Contractors Association of Alberta (MCAA), the Canada Masonry Design Centre (CMDC), the Canadian Masonry Producers Association (CCMPA), the Natural Sciences and Engineering Research Council (NSERC) Collaborative Research and Development Grant program, and the National Council of Science and Technology (CONACYT).

Finally, I would like to thank the people at Scorpio Masonry in Edmonton for their patience with the project and for sharing their expertise during this work.

TABLE OF CONTENTS

LIST OF TABLES

LIST OF FIGURES

1 INTRODUCTION

1.1 Background

Reinforced concrete masonry walls are commonly chosen as the preferred building system in single-storey structures such as school gymnasiums, retail stores, and industrial and commercial warehouses.. The reasons are that they provide the structure and the skin simultaneously, fire and sound resistance are built right into the wall, and the result is aesthetically pleasing. Additionally, the mentioned benefits are provided in a cost-effective solution.

From the 1950s, the construction of big supermarkets, particularly on the west coast of the United States, pushed for the use of walls taller than the 4.9 m allowed for 200 mm blocks. Due to this trend, concrete tilt-up panels became popular, and designers realized the lack of comprehensive design criteria for tall walls. Motivated by the need to exceed the code limitations of height-to-thickness ratio and to investigate long-term serviceability, the American Concrete Institute (ACI) and the Structural Engineers Association of Southern California (SEASC) published a Test Report on Slender Walls in 1982. A series of 7.4 m walls with height-to-thickness ratios of 29 and larger were tested under combined axial and out-of-plane loads. This report was used as a reference in developing masonry design standards in North America (CSA S304-14; TMS 402-16). The experimental constraints present in the SEASC testing program translated into limitations imposed by such standards, as all the walls had relatively small axial loads, were under-reinforced and were tested in a pinned base condition.

Current provisions in North American masonry standards, such as the Canadian CSA S304-14 and the American TMS 402-16, require walls with a slenderness ratio (kh/t) of 30 or greater to satisfy stringent requirements like assuming a pinned support at the base and limiting the compressive axial load. For a 200 mm block wall, the most commonly used size, this would mean a maximum height of 5.7 m to be considered non-slender and avoid the additional restrictions. For reference, most warehouses built in recent years had ceiling clearances of 8.4 to 10.8 m. The susceptibility of slender walls to second-order (P-Delta) effects is the reason for the mentioned requirements since it is believed that these walls have early instability issues. However, there is no evidence to justify these assumptions, and recent studies show that design standards are overly

conservative. Moreover, the drastic decrease in capacity at a slenderness ratio of 30 set in the standard, from 80% to 10%, is an approach only used in masonry. For instance, the concrete design standard A23.3-14 uses a factor that is a continuous function of slenderness. For masonry, this means that slender walls quickly require the use of thicker units during the design process. Thicker masonry units lead to more expensive walls since they present greater material costs, need more time and effort from masons and use more space from the project.

Additionally to the ACI-SEASC study, a few other experimental programs on slender walls have been conducted (Yokel et al., 1971; Hatzinikolas, 1978; Hamid et al., 1989; Liu and Dawe, 2001). The majority of them focused on using pin-pin support conditions until Mohsin and Elwi (2003) investigated the role of non-zero rotational base stiffness on masonry walls. Some of these studies tested walls with a height-to-thickness ratio over 30 but did not recreate conditions found in real practice, such as clear height or out-of-plane loading.

One of the most critical elements in the process of designing slender masonry walls is the evaluation of second-order effects. Second-order effects are determined by calculating the total applied moment on the wall, comprised of first-order and second-order moments. First-order moments for loadbearing masonry walls usually come in the form of vertical loads acting at an eccentricity, applied lateral loads, or a combination of both. Second-order moments are caused by the out-of-plane displacement of the wall from by first-order moments, creating additional eccentricity between the wall and the vertical load. This additional moment increases the total out-of-plane displacement, which then increases the second-order moment. This phenomenon is also called P-Delta effect.

Slender masonry walls are particularly sensitive to second-order effects due to the large out-of-plane displacements they experience during loading. Several techniques have emerged to overcome this issue, placing the reinforcement farther from the neutral axis to increase the out-of-plane stiffness of reinforced masonry walls, thus reducing the influence of second-order effects (Abboud et al., 1996; Korany and Drysdale, 2006; Sparling and Palermo, 2021). Some other solutions exist to enhance reinforced masonry wall stiffness, such as the use of in-line boundary elements (Entz 2017) and post-tensioning the vertical reinforcement (Popehn et al., 2007)

1.2 Objective

The objective of this study is to characterize the response of a typical slender partially-grouted concrete-masonry wall under a combination of axial and out-of-plane loads. To achieve this, the following tasks need to be completed:

1. Conduct a literature review to understand the techniques available to analyze the response of slender masonry walls and the research efforts to get rational design criteria for such walls during the last 50 years.
2. Develop and validate, based on previous studies, a computer-based numerical model to predict the behaviour of slender masonry walls under axial and out-of-plane loads.
3. Design and build an innovative test setup capable of testing 8.75 m wall specimens under a combination of axial and out-of-plane loads.
4. Conduct a test of an 8.75 m wall with a height-to-thickness ratio of 46 and pin-pin supports, subject to a sustained eccentric vertical load, representing the gravity loads coming from the roof system, and an increasing out-of-plane load representing wind pressure applied to the wall. The design of the wall should be representative of a typical wall found in practice.
5. Use test results to calibrate the numerical model and generate recommendations for future tests on slender masonry walls.

The results from this experimental program will serve as a reference for future tests using the same test setup presented in this study. The goal of this and the future tests of this research program is to assess the performance of the current Canadian masonry design standard for slender masonry walls and generate a rational design procedure that takes advantage of modern analysis tools.

1.3 Scope

The scope of this research is limited to the flexural assessment of a partially grouted slender masonry wall. Shear failures of flexural walls are not considered in this study. The numerical model proposed in this study is a 2-D finite element model, using a simplified section and a macro-modelling approach. Therefore, it can only estimate the overall response of walls. Only walls built with hollow concrete masonry units were assessed in this thesis. The test setup designed for this study was assumed to be stiff enough to neglect any displacements relative to the specimen when loads were applied. The experimental program was limited to one wall with a typical reinforcing

configuration due to experimental constraints. The wall was designed following CSA S304-16 provisions for slender masonry walls, with non-seismic specifications. The wall was loaded until vertical reinforcement presented yielding, not to failure, due to safety concerns. A forensic investigation on the wall tested is recommended but out of the scope of this study.

1.4 Thesis organization

This thesis is divided into five chapters, and their content is described as follows:

Chapter 1: Presents an introduction to the problem investigated, and the objectives and scope of this study are discussed.

Chapter 2: Presents a review of the literature available, including full-scale wall tests and numerical studies, as well as an overview of some North American and European masonry design standards, to get an understanding of slenderness effects in modern masonry walls. This chapter addresses Task 1.

Chapter 3: Describes the implementation of a numerical model to estimate the response of RM walls subject to a combination of axial and out-of-plane loads. Validation of this model is also presented along with a new proposal to enhance the flexural stiffness of these walls. Chapter 3 completes Task 2.

Chapter 4: The experimental program is described, including the design of a special test setup, the construction process for the specimen and the results obtained. This chapter addresses Tasks 3, 4 and part of Task 5.

Chapter 5: Summarizes the conclusions drawn from this study and a series of recommendations for future studies on this topic. Chapter 5 discusses the rest of Task 5.

2 LITERATURE REVIEW

2.1 Introduction

This chapter presents an overview of techniques available to analyze the response of Slender Masonry Walls (SMW) and research efforts to get rational design criteria for SMW, in the form of analytical studies and test programs during the last 50 years. Also, a brief description of the current code and standard requirements in Canada, as well as in the United States and Europe. These design standards have been shown to be overly conservative by several researchers. Therefore, there is a need to implement rational design procedures based on evidence from full-scale tests. Since the main problem with slender walls is the large influence of second-order effects on their structural behaviour, it is imperative to implement solutions to increase the flexural stiffness of these walls as a means to get more efficient designs. In this tone, some techniques for stiffening SMW are presented in section 2.5. Lastly, the current needs in research to get a complete understanding of the behaviour of SMW are described.

2.2 Mechanics of Slender Walls

The mechanics of slender concrete columns and a revision of design procedures were presented by MacGregor et al. (1970). In essence, a short column is that with a strength equal to or greater than that computed for its cross-section for a combined moment and axial load, and a slender column is that with a strength reduced by second-order effects.

The effect of slenderness on a column is illustrated in Figure 2.1. Two types of failure can occur: a material failure, illustrated by column 1 in Figure 2.1, where axial load P and moment M exceed the strength of the cross-section; and a stability failure, illustrated by column 2 in Figure 2.1, where the column reaches a deflection (Δ_2) due to axial force P and end moment Pe, such that the value of $\delta M/\delta P$ is zero or negative. This type of failure may occur in slender columns (MacGregor et al., 1970).

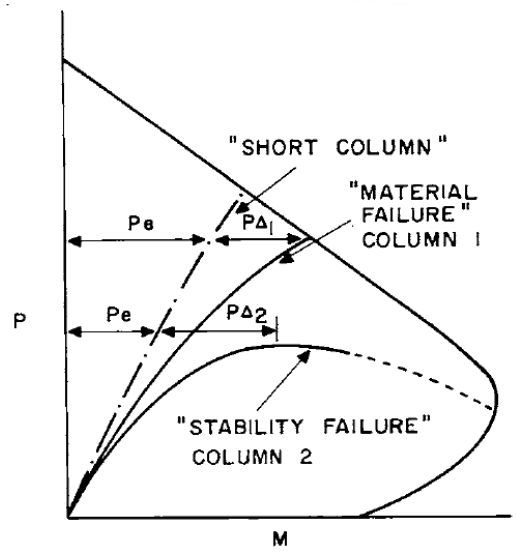

Figure 2.1: Load and moment interaction in concrete columns (MacGregor et al., 1970).

The same principles apply to masonry walls. The axial capacity of a wall decreases as slenderness increases, as illustrated in Figure 2.2. In masonry, slenderness is defined as the height-to-thickness ratio, kh/t, where the effective height factor k accounts for end conditions at the top and bottom of the wall. Effective length factors for masonry walls and columns can be found in Annex B of S304. For slender walls, this decrease in capacity is associated with buckling (Drysdale and Hamid, 2005; Sandoval et al., 2011). A slender wall, straight and concentrically loaded, will fail in buckling if the compressive strength of the material is not exceeded by the critical stress.

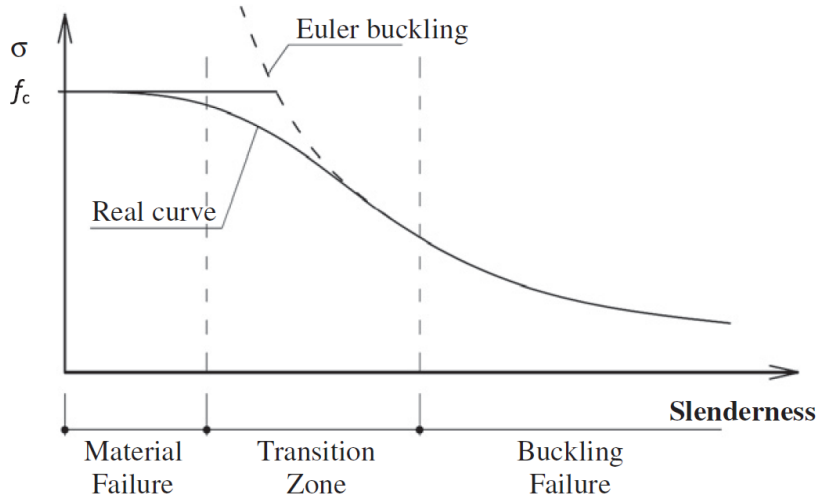

Figure 2.2: Effect of slenderness on compressive stress (σ) capacity (Sandoval et al., 2011)

In real walls, loads are eccentrically applied, even just by accounting for imperfections in the wall. This eccentric load induces a moment that may lead to tensile stresses in the cross-section. Due to the low tensile strength of masonry (~0.65 MPa), which mostly depends on the bond between block and mortar, tensile cracks appear under relatively small moments. The extent of cracking is dependent on the eccentricity of the applied load, the magnitude of the load and the lateral deflection (Hatzinikolas et al., 1978). As the load increases, out-of-plane displacements increase, and the eccentricity in the central portion of the wall increases, as shown in Figure 2.3. A reinforced masonry wall will exhibit the mentioned behaviour until the crack reaches the location of the reinforcement (Hatzinikolas et al., 1978).

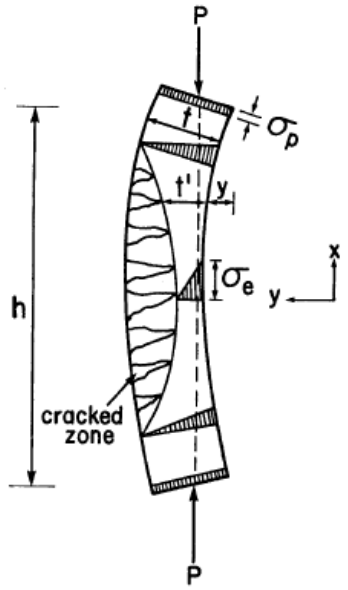

Figure 2.3: Deflected shape of an eccentrically loaded unreinforced wall (Hatzinikolas et al., 1978).

According to research (Yokel et al., 1971; Hatzinikolas et al., 1978; Sandoval et al., 2011), many factors such as the location and amount of reinforcement, rotational restraint at supports, masonry tensile strength, masonry's nonlinear stress-strain relationship, the extent of cracking, and long-term creep and shrinkage all contribute to slenderness effects. This makes establishing wall response to slenderness very complex.

One of the most critical elements in the process of designing slender masonry walls is the determination of second-order effects (Petit, 2019). Second-order effects are determined by calculating the total applied moment on the wall, composed of first-order and second-order

moments. First-order moments for loadbearing masonry walls usually come from vertical loads acting at an eccentricity, applied lateral loads, or a combination of both. Second-order moments occur when the out-of-plane displacement of the wall caused by first-order moments creates an eccentricity between the wall and the vertical load. This additional moment increases the total out-of-plane displacement, which then increases the second-order moment. This phenomenon is also called P-Delta effect. SMW are particularly sensitive to second-order effects due to the large out-of-plane displacements they experience during loading.

The Canadian standard for masonry design S304-14 and the American code for masonry structures TMS 402-16 permit two methods for evaluating second-order moments for slender masonry walls: The load-displacement or $P\delta$ method and the moment magnifier (MM) method. The $P\delta$ method determines the total moment, including second-order moments, through iteration until convergence is reached (otherwise, the structure may be unstable). The MM method involves the magnification of the maximum first-order moment by a factor to estimate the maximum total moment in an element. This method was introduced by MacGregor et al. (1970) for slender concrete columns and is valid for members in single curvature with the location of the primary maximum bending moment coinciding with the location of the total maximum bending moment. The MM method determines the total moment in a single calculation, making it easier for designers. Equations and the procedure for both methods are presented in section 2.4.

2.3 Research on Slender Masonry Walls

Modern research on full-scale SMW started in the 1970s, when Yokel et al. (1970) tested 60 reinforced and unreinforced Concrete Masonry Walls (CMW) with concentric and eccentric vertical loads and slenderness ratios from 15 to 40. Their objective was to determine and analyze the effects of wall slenderness and load eccentricity on the strength of CMW. This study highlighted the need for a rational method to design SMW, considering not only the height-to-thickness ratio but also variables such as end fixity, cross-section properties, and the modulus of elasticity of the masonry. In 1971, Yokel et al. tested 90 unreinforced masonry walls. Specimens were 2.44 m tall, varying from 12 to 24 in slenderness ratio. Researchers reported that the cross-sectional moment capacity of a wall was conservatively predicted by a theoretical interaction curve

based on compressive prism strength and linear strain gradients and that the Moment Magnifier (MM) method closely predicted the slenderness effects for the tested walls.

In an experimental study by Hatzinikolas (1978), sixty-eight full-scale CMW with slenderness ratios from 12 to 22 were subject to various eccentric loads. All walls were tested with pin-end conditions. A MM method was proposed utilizing effective rigidity to evaluate the effect of slenderness on the capacity of CMW.

With the increased use of masonry walls for industrial and commercial buildings through the 1970s, there was a trend toward having more slender walls to save on costs and increase usable building space (Hatzinikolas, 1978; ACI-SEASC, 1982). To evaluate the then-current design process and slenderness limitations, the ACI-SEASC task committee tested 30 full-scale slender walls (Figure 2.4). These panels were built using tilt-up reinforced concrete, clay bricks, clay hollow blocks and hollow concrete blocks. Nine of them were Fully Grouted (FG) Reinforced Masonry (RM) walls. All specimens were 7.4 m high, with slenderness ratios from 30 to 52. A welded steel truss frame was designed and built for this purpose. Lateral loads were supplied by an airbag attached to the frame and installed on the back of the panels. Vertical loads were applied using a lever system installed on the top of the frame. For all walls, eccentricity was equal to the half-thickness of the specimen plus 76 mm.

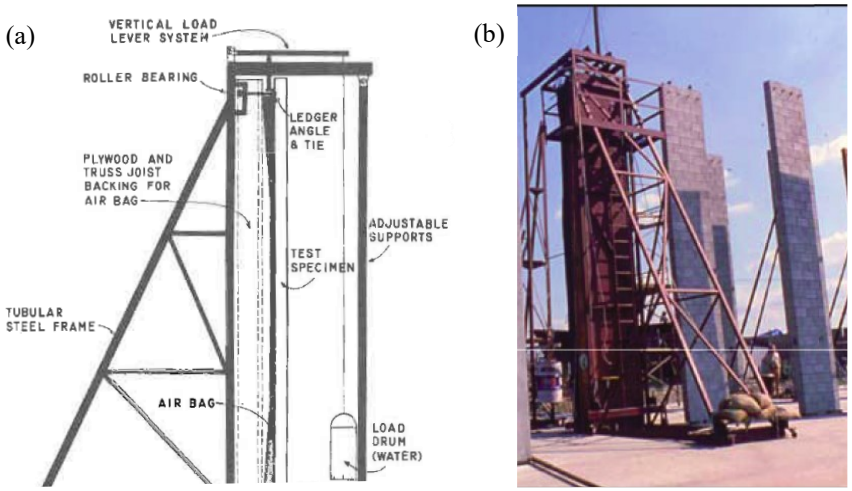

Figure 2.4: Slender walls test program (a) Side elevation of the test setup (b) Loading frame next to ready-to-test walls (ACI-SEASC, 1982).

Dimensions of the nine RM walls, along with vertical load values and ratios, are presented in Table 2.1. Vertical load ratios are calculated by dividing the load applied by the axial compressive strength of the cross-section. All measures were taken to allow free rotation at both the bottom and top supports, thus creating pin-pin boundary conditions.

Table 2.1: Dimensions and loads of RM walls tested. (ACI-SEASC, 1982).

Wall ID	Thickness, mm	h/t Ratio	Vertical Load, kN/m	f'm, MPa	Vertical Load Ratio, %
1	245	30	4.67	16.96	0.09
2	245	30	12.55	16.96	0.25
3	245	30	12.55	16.96	0.25
4	194	38	12.55	17.89	0.3
5	194	38	12.55	17.89	0.3
6	194	38	4.67	17.89	0.11
7	143	52	4.67	21.96	0.12
8	143	52	4.67	21.96	0.12
9	143	52	4.67	21.96	0.12

In the Test Report, published in 1982, it was concluded that there was no evidence of elastic and inelastic lateral instability at the load ranges tested. It was also shown that fixed height-to-thickness limits in design standards were not valid. The study recommends using deflection limits to control residual deflection in walls after noting a permanent deflection for panels loaded to the yield level of reinforcement.

Hamid et al. (1989) tested fourteen 2.4 m tall CMW under monotonic and cyclic out-of-plane (OOP) lateral loads. The objective was to evaluate the effects of parameters such as percentage and location of vertical steel, block size, the extent of grouting, and load pattern on the wall behaviour. In this study, all walls had two vertical bars centrally located, except for one wall with staggered reinforcement. Details of the cross-sections are shown in Figure 2.5. It was observed that increasing the percentage of vertical reinforcement largely increased the load capacity of the walls and that the staggered-bars configuration produced larger capacity and ductility.

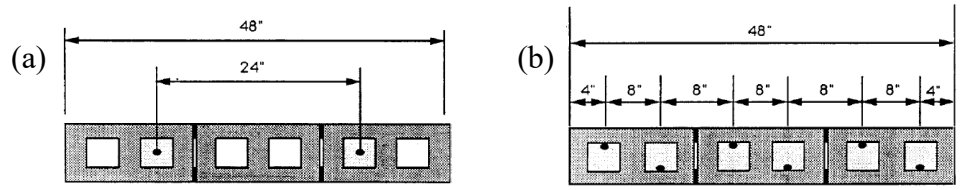

Figure 2.5: Location of vertical reinforcement in masonry walls (a) Rebar at the centre (b) Rebar staggered (Hamid et al., 1989).

In 2001, Liu and Dawe performed tests on 36 RM walls. All specimens were 1200 mm high, with a slenderness ratio of 8.6, pin supported, and subject to combined axial and lateral load. Results indicated that the current standards underestimated the effective stiffness of masonry walls failing primarily by compression and that E_m may also be dependent on the level of axial compression. Similar conclusions were drawn by Liu and Hu (2007) after testing 12 RM walls with a height of 2.4 m. All specimens were in pin-pin conditions with a slenderness ratio of 17.1. The results corroborated that the moment magnifier method used in the standards was effective, but EI_{eff} was underestimated. Calculating EI_{eff} by S304 predicts ultimate capacities between 51-63% of the test results. However, a proposed EI_{eff} calculation along the use of the Moment Magnifier (MM) method provided estimations in good agreement with test results. More recently, Müller et al. (2017) examined test results reported by different researchers and compared them against the estimations in the Canadian standard. It was concluded that S304 predictions are especially conservative with increasing wall heights and decreasing load eccentricities. This is mainly due to the underestimation of the effective flexural rigidity.

The majority of investigations on RM walls subject to axial and out-of-plane loads focused on using pin-pin boundary conditions until Mohsin and Elwi (2003) conducted full-scale testing of CMW with slenderness ratios of 28.6 and 33.9 and investigated the role of non-zero rotational base stiffness on loadbearing masonry walls. A numerically estimated rotational stiffness, based on field-based parameters of real foundations, was applied at the support of the walls using the test setup shown in Figure 2.6a. Results showed a consistent effect of the rotational stiffness at the base on the buckling behaviour of these walls, hence demonstrating that support stiffness controls the effective length of the walls and their effective stiffness. Isfeld et al. (2019) investigated the effect of the base support conditions on the deflected shape on Partially Grouted (PG) CMW. Three 2400 mm

tall walls, with slenderness ratios of 10.2 and 12.6, were subjected to axial and out-of-plane loading. The test setup used to recreate both pinned and fixed base conditions is shown in Figure 2.6b. The results of these tests were then compared with calculations based on the Canadian masonry standard. This comparison exhibited that a pinned support condition is not an accurate representation of real practice.

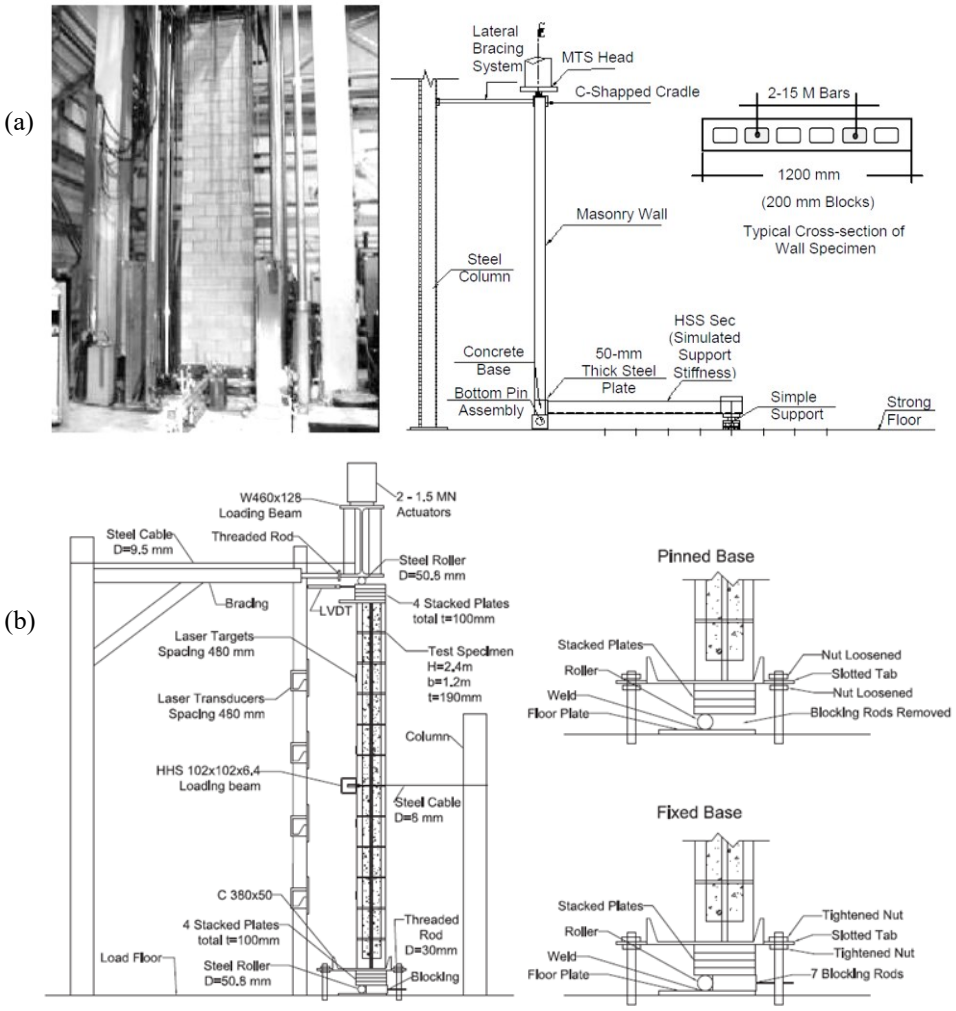

Figure 2.6: Test setup and specimen details to evaluate the effect of the base support condition on RM walls (a) Mohsim and Elwi, 2003 (b) Isfeld et al., 2019

Similar efforts to challenge boundary conditions imposed by the codes were made in Europe when Da Porto et al. (2011) built two sets of 6 m high RM walls connected at the top by a heavy slab (Figure 2.7). The slab was hinged to transfer horizontal displacements to both walls while allowing free rotation. Walls were fixed to the base and had a slenderness ratio of 15.8. In these cantilever boundary conditions, lateral out-of-plane cyclic displacements with increasing amplitude were

applied, followed by a final monotonic load. Results are also presented from a numerical model assessing the response of these structures. This study concludes that slenderness limits imposed by the Eurocode, as well as assuming simply-supported walls, are too conservative when compared with experimental and numerical results.

Figure 2.7: Test setup for cyclic out-of-plane testing on RM walls (da Porto, 2011).

In a different approach to evaluating the out-of-plane stability provisions in the Canadian standard used in the design of shear walls, Robazza et al. (2018) presented the results of five slender RM walls under in-plane reversed-cyclic loading. The walls tested, with slenderness ratios from 21 to 29, failed in in-plane shear without exhibiting signs of out-of-plane instability.

An overview of experimental programs that tested masonry walls under axial loads, out-of-plane loads, or a combination of both is presented in Table 2.2.

Table 2.2: Experimental programs on the out-of-plane behaviour of masonry walls.

Study	Walls	Type	Grout	Height, m	h/t	f'm, MPa	Reinf. ratio, %	Load protocol	End conditions
Yokel et al. (1970)	60	UR, R	PG	3.1 - 6.1	16 - 43	13.03	0.23	Concentric or eccentric axial load applied to failure	P - F
Yokel et al. (1971)	90	UR	-	2.5	13	5.3 - 12.34	-	Axial load applied on top, then incremental OOP load by inflating airbag to failure	P - PF
Hatzinikolas et al. (1978)	68	UR, R	PG	2.7 - 4.7	12 - 22	12.61	0.1 - 1	Concentric or eccentric axial load applied to failure	P - P
ACI-SEASC (1982)	9*	R	FG	7.4	30, 38, 52	16.96, 17.89, 21.96	0.22 - 0.37	Axial load applied at eccentricity of t/3 + 75 mm, then incremental OOP load by inflating airbag (no failure)	P - P
Hamid et al. (1989)	14	R	FG, PG	2.4	12, 16, 21	10.48 - 14.13	0.15 - 0.44	Monotonic or cyclic out-of-plane loads to failure	P - P
Liu and Dawe (2001)	36	R	PG	1.2	8.6	17	0.18 - 0.36	Concentric axial load applied on top, then incremental OOP load at midspan to failure	P - P
Mohsin and Elwi (2003)	8	R	PG	5, 6	29, 34	12	0.17	Axial load at an eccentricity of t/3 applied on top to failure	P - P, P - PF
Liu and Hu (2007)	12	R	PG	2.4	17	15 - 17.3	0.18	Axial load at different eccentricities applied on top to failure	P - P
Da Porto et al. (2011)	4	R	PG	6	16	-	0.1 - 0.2	A heavy slab was hinged at the top and used to transfer cyclic horizontal displacements	C
Isfeld et al. (2019)	3	R	PG	1.2	10, 13	15.22	0.18	Combination of eccentric axial load and out-of-plane load, both applied at specific magnitudes (no failure)	P -P, P - F

UR = unreinforced, R = reinforced, PG = partially grouted, FG = fully grouted, P = pinned, F = fixed, PF = partially fixed, C = cantilever
* Only counting concrete masonry walls

2.4 Design Standards

The Canadian masonry standard CSA S304-14 in clause 10.7.3.3 presents the following categories regarding the slenderness of walls:

- Slenderness effects are ignored when $^{kh}/_{t} < 10 - 3.5(^{e_1}/_{e_2})$
- Slenderness effects are considered if $10 - 3.5(^{e_1}/_{e_2}) < {}^{kh}/_{t} < 30$. Either the $P\delta$ or MM method shall be used to design the wall.
- If $^{kh}/_{t} > 30$, additional provisions apply.

Where k is the effective length factor, h is the wall height, t is the wall thickness, and e_1 and e_2 are the eccentricities at the top and bottom supports, respectively.

In the last two groups, second-order effects are accounted for in the determination of the total factored moment (M_{ftot}). Clause 10.7.4.2 presents the $P\delta$ method using Equation (2.1).

$$M_{ftot} = M_{fp} + P_f \delta_f \tag{2.1}$$

Where M_{fp} is the factored primary (i.e. first-order) moment, P_f is the factored axial load, and δ_f is the out-of-plane displacement of the wall at the critical section under axial and lateral loads, including second-order effects. This method naturally takes the designer to an iterative procedure until convergence is achieved; if convergence is not achieved, then the wall is not stable. A simpler procedure is presented in the MM method, where the total moment is determined with Equation (2.2). This factored total moment can not be less than the factored primary moment due to end moments and lateral loads.

$$M_{ftot} = M_{fp} \frac{C_m}{1 - \frac{P_f}{P_{cr}}} \tag{2.2}$$

Where C_m is a factor relating the actual moment diagram to an equivalent uniform moment diagram, and P_{cr} is the critical axial compressive load. C_m is calculated using Equation (2.3) and shall not be less than 0.4.

$$C_m = 0.6 + 0.4 \, {}^{M_1}/_{M_2} \tag{2.3}$$

Where M_1 and M_2 are moments at each end of the wall. If eccentricities at both ends are equal to or less than $0.1t$ then M_1 / M_2 must be taken as equal to 1.0.

And P_{cr} is calculated using Equation (2.4).

$$P_{cr} = \frac{\pi^2 \phi_{er} E I_{eff}}{[(1 + 0.5\beta_d)(kh)^2]} \tag{2.4}$$

Where $\phi_{er} = 0.75$ for reinforced masonry (Clause 4.3.4 of S304), β_d is the ratio of factored dead load moment to total factored moment, and EI_{eff} is the effective flexural stiffness of the wall. In lieu of more detailed calculations, S304 requires the use of Equation (2.5). If determined by alternate methods, these should consider the influence of axial loads, variable moments of inertia, and material nonlinearities.

$$EI_{eff} = E_m \left[0.25 I_o - (0.25 I_o - I_{cr}) \left(\frac{e - e_k}{2e_k} \right) \right] \tag{2.5}$$

Where E_m is the modulus of elasticity of masonry, I_o is the moment of inertia of the effective cross-sectional area, I_{cr} is the transformed moment of inertia of the cracked section, e is the axial load eccentricity and e_k is the kern eccentricity for the effective cross-sectional area. Values for e and e_k are calculated using Equations (2.6) and (2.7), respectively.

$$e = \frac{M_{fp}}{P_f} \tag{2.6}$$

$$e_k = \frac{S_e}{A_e} \tag{2.7}$$

Where S_e is the section modulus of the effective cross-sectional area, and A_e is the effective cross-sectional area of masonry including the mortar bedded area and the area of voids filled with grout.

For walls in the last category (with $^{kh}/_{t} > 30$) both the $P\delta$ and the MM methods may be used. Additionally, clause 10.7.4.6 of S304-14 imposes the following requirements:

- Walls shall be constructed with masonry units 140 mm or more in thickness
- Pinned conditions must be assumed at each end of the wall
- The factored axial load can not exceed $0.1\phi_m f'_m A_e$
- To guarantee a ductile response, the vertical reinforcement provided shall be less than or equal to that provided by the condition $\frac{c}{d} \leq \frac{600}{600+f_y}$

Where ϕ_m is the resistance factor for masonry provided by S304, f'_m is the compressive strength of masonry, c is the distance from an extreme compression fibre to the neutral axis, d is the distance from an extreme compression fibre to the centroid of vertical reinforcement, and f_y is the yield strength of vertical reinforcement.

The total factored moment, determined at the mid-height of the wall, shall be calculated using Equation (2.8).

$$M_{ftot} = \frac{w_f h^2}{8} + P_{ft}\left({}^{e}/_{2}\right) + \left(P_{fw} + P_{ft}\right)\Delta_f \tag{2.8}$$

Where w_f is the factored uniform lateral wind load on the wall, P_{ft} is the factored vertical load from the tributary roof area, P_{fw} is the factored weight of the wall above midspan, e is the

eccentricity of the vertical load, and Δ_f is the lateral deflection of the wall at mid-height under factored lateral or axial loads including effects of second-order moments. This equation is based on a single-storey wall with pin-pin conditions. Alternatively, S304 allows for the use of Equation (2.2) to compute M_{ftot} using $Cm = 1.0$ and $k = 1.0$.

Provisions in the U.S. masonry code TMS 402-16 regarding SMW are similar to those in the Canadian standard. Clause 9.3.5 sets the requirements for the design of walls for out-of-plane loads. Clause 9.3.5.4.2 states that the design moment (M_u), calculated at the mid-height of the wall, may be determined by a $P\delta$ method using Equation (2.9).

$$M_u = \frac{w_u h^2}{8} + P_{uf}\frac{e_u}{2} + (P_{uw} + P_{uf})\delta_u \tag{2.9}$$

Equation (2.9) is essentially the same as Equation (2.8), where variables were defined earlier. For this procedure, simple supports are assumed at the top and bottom of the wall. The compressive stress due to the axial load must not exceed $0.2f'_m$. If the ratio of effective height to nominal thickness, h/t, exceeds 30, the compressive stress due to the axial load must not exceed $0.05f'_m$.

An alternative method to calculate M_u is presented in clause 9.3.5.4.3, stating that the design moment may be determined by a second-order analysis or by a first-order analysis and a moment magnifier parameter using Equation (2.10). This equation is very similar to Equation (2.2) from S304, and a similar process to compute each variable is detailed in the TMS 402 code.

$$M_u = M_{u0}\frac{1}{1 - \frac{P_u}{P_e}} \tag{2.10}$$

The test setup and boundary conditions used by the SEAOSC researchers in 1982 may have influenced the above provisions in the standards (both Canadian and American) related to the design of SMW. Requirements for minimum block thickness, ductile steel yielding, a maximum slenderness ratio of 30, limiting the axial load and always assuming a pinned support all resemble the conditions of the mentioned study. However, more recent research shows that these provisions need to be re-evaluated to allow for a more efficient design in RM walls.

Bilotta Rios and Cruz Noguez (2021) presented a numerical study to assess the method in North American standards to estimate second-order effects in RM walls. It was shown using numerical simulations that second-order effects calculated using CSA S304-14 are overly conservative. Following the TMS 402-16 provisions resulted in an acceptable percentage of error up to a slenderness ratio of 40, but the error grew gradually for higher ratios. The study also proposed a new equation to estimate the effective stiffness of RM walls. This and the use of the MM method results in a better alternative to estimate the second-order effects for walls subject to compressive and OOP loads under pinned-pinned conditions.

To date, most building codes and standards do not present a consistent approach for calculating second-order effects in masonry structures. For instance, the Italian and European codes do not consider them explicitly but set slenderness limits for pin support conditions at both ends without providing alternative rational design procedures. The Italian code (DM 14/01/08) provides a height-to-thickness limit (λ_{lim}) of 20 for masonry structures and 15 for RM walls in seismic areas. For all elements, second-order effects are implicitly introduced into the verification procedures for vertical loading. Eurocode 6 (EN 1996-1-1) sets a maximum value of $\lambda_{lim} = 27$ for RM walls, but any wall above $\lambda_{lim} = 12$ shall be designed according to the requirements for Unreinforced Masonry Walls (URM) and taking into account second-order effects by an additional design moment. None of these procedures provide designers with correct estimates of actual second-order effects and result in extremely conservative designs (da Porto et al., 2011; Donà et al., 2018). After presenting a numerical study using OpenSEES, Donà et al. (2018) proposed a new slenderness limit of 40 for the design of RM walls for commercial and industrial buildings. Although construction practices and materials in Canada and Europe are not the same, it is evident that there is a similar problem of a lack of modern procedures to evaluate the response of SMW in the current standards.

Of the mentioned requirements for the design of SMW, the most restrictive may be both the assumption of pinned end conditions and the limitation of flexural reinforcement. Designers often calculate second-order effects using the moment magnification method, a method in which a factor amplifies the primary moment to account for the additional moments created by the vertical load on a deflected profile. Determination of this moment magnification factor heavily depends on the

effective flexural rigidity (EI_{eff}) and the effective length factor (k). The current underestimation of the effective flexural rigidity and the imposed assumption of pinned end conditions ($k = 1.0$) greatly increases the moment magnification factor, resulting in a large amplification in the design moment of the wall. A design solution could be to increase the steel reinforcement in the wall cross-section; however, this additional steel may then violate the provision that requires SMW to fail with a ductile behaviour. If this is the case, designers are then forced to use a larger masonry unit, resulting in an uneconomical design.

2.5 Stiffening techniques

In conventional RM wall construction, steel rebar is placed at the centre of the wall cross-section, as shown in Figure 2.8. This practice results in inefficient use of reinforcement because it is close to the out-of-plane neutral axis (NA).

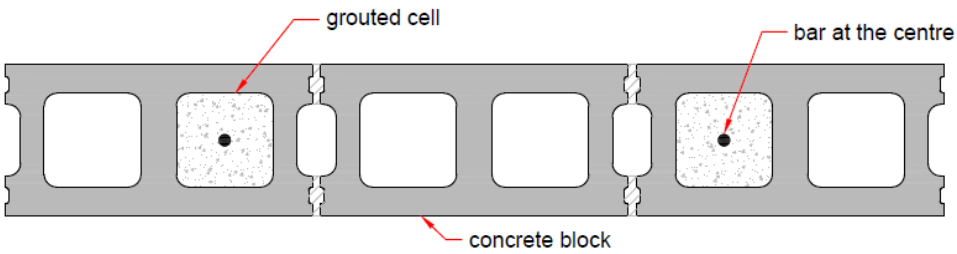

Figure 2.8: Typical position of the vertical reinforcement in masonry walls construction.

To overcome this issue, several techniques have emerged placing the reinforcement farther from the NA to increase the out-of-plane stiffness of RM walls. This results in stiffer walls, which reduce second-order effects, without the use of thicker and heavier CMUs (Concrete Masonry Units). A simple example of this was proposed by Abboud et al. (1996), where the reinforcing bars within the cells were located as near to the inner side of the face shell as practicable, as shown in Figure 2.9. In this study, six panels 2.64 m high with slenderness ratios between 17.4 and 23.1 were tested to determine the effects of percentage and location of vertical reinforcement, block size and extent of grouting on the behaviour of RM walls under out-of-plane monotonic loading. Results showed that the percentage and location of vertical bars had a significant effect on the stiffness of the wall. However, recommendations on clear spacing and ductility behaviour provided in Canadian standards prevent, to some extent, the use of these solutions.

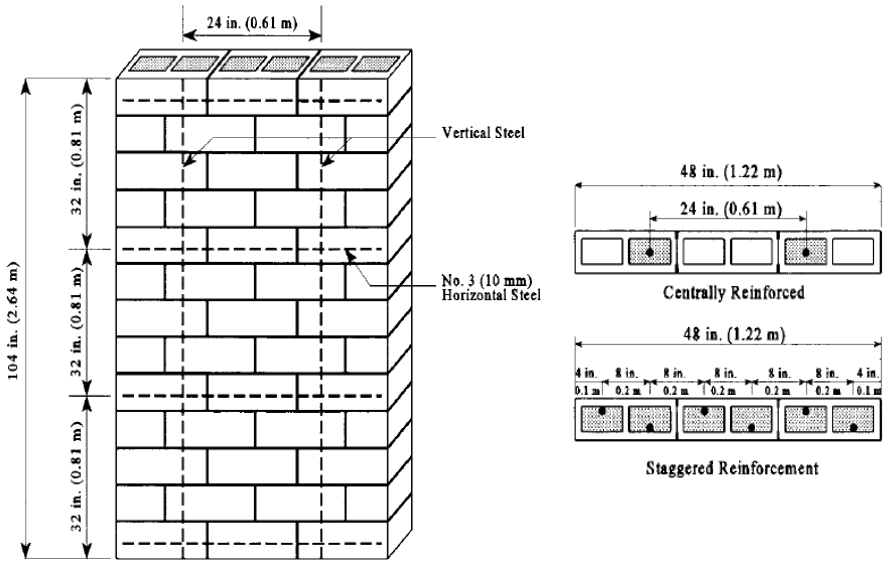

Figure 2.9: Specimen details of RM walls to test under out-of-plane loads (Abboud et al., 1996).

Near-surface mounted (NSM) reinforcement is a technique where reinforcement is adhered to the extreme fibres of a structural element to increase strength and stiffness. NSM reinforcement has been extensively used to retrofit structures to increase their resistance before changing loading conditions or to improve seismic resilience by cutting grooves into walls and placing the reinforcement with epoxy or cementitious material. The state of practice is well documented by De Lorenzis and Teng (2007).

Korany and Drysdale (2006) explored the use of unobtrusive fibre-reinforced polymer (FRP) rehabilitation techniques mounted near the surface of the façade walls in epoxy-filled grooves. Ten full-scale unreinforced walls built of clay bricks and retrofitted with the developed techniques were tested under both monotonic and cyclic loads. Walls achieved a significant increase in ultimate capacity and stiffness. Sparling et al. (2018) introduced a new Surface Reinforced (SR) CMU with a pair of channels on the external faces to include NSM reinforcement during the construction of new walls (Figure 2.10). Enough units were fabricated to build a series of 3.2 m tall by 1.2 m wide panels. Results showed that RM walls with NSM reinforcement using the same steel ratio have higher strength and stiffness than those with a conventional configuration. In an effort to understand the response of slender RM walls under service loading conditions, Sparling and Palermo (2021) designed a loading frame to test simply supported 8m-tall RM walls in combined axial and out-of-plane conditions. Cyclic testing on a (PG) wall with conventional reinforcement

configuration exhibited increasing moment resistance and decreasing out-of-plane load capacity with increasing axial loads. This wall is the first of a testing program that will compare the behaviour of walls with conventional embedded steel bars to a series of walls with Near-Surface Mounted (NSM) reinforcement. Despite all the structural advantages, this innovative system may come with challenges related to installation times and structural fire safety.

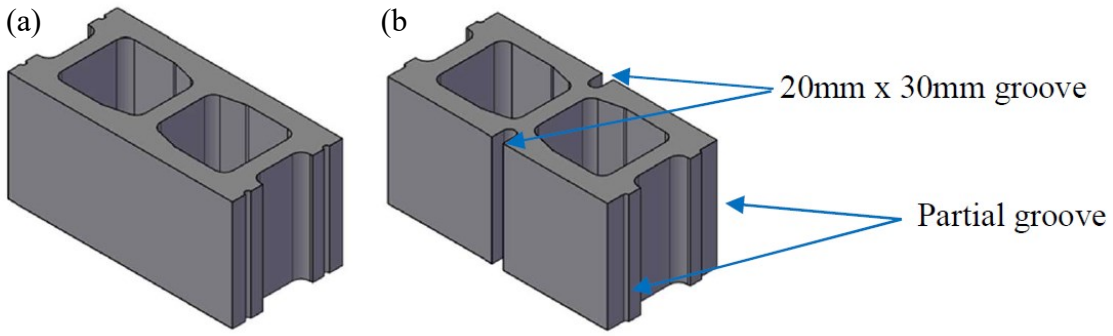

Figure 2.10: CMU types for NSM RM walls study (a) Conventional unit (b) Specialty unit with grooves on face shell (Sparling and Palermo, 2021)

Entz et al. (2017) improved the reinforcement scheme inside the blocks with pre-tied steel cages with specially designed CMUs that can slide around the cage to form an in-line boundary element, as shown in Figure 2.11. In this system, the increase in the moment arm of the reinforcement played a major role in reducing OOP deflections in loadbearing RM walls. This system enhanced the pre-cracked response, but after cracking, the flexural stiffness of the enhanced wall and the conventional wall started to converge. The primary mechanism by which the OOP stiffness is enhanced is by inducing a compressive force in the rebar layer placed in the compression zone. Therefore, this method is better suited for high axial load conditions.

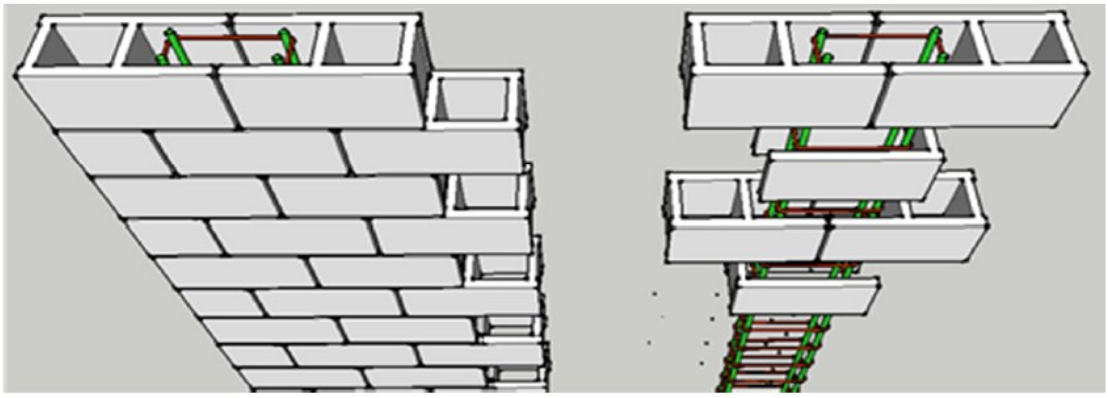

Figure 2.11: Schematic of RM wall built using the in-line boundary elements (Entz, 2017).

Another method to restrict the out-of-plane bending includes post-tensioning the main vertical reinforcement. Using this technique, precompression stresses on the masonry offset the tensile stresses experienced under service conditions. This is most beneficial when axial loads are low and out-of-plane loads, such as wind pressure, are significant (Popehn et al., 2007).

2.6 Gaps in research

Based on the analysis of the previously presented studies, further testing is needed to provide results for the proposal of a less conservative design for SMW. The assumption in the standards about slender walls being inherently unstable and requiring special restrictive design provisions should be re-evaluated.

The majority of researchers have tested walls with pinned support conditions at the bottom and the top of the panels. In practice, masonry walls are built on a foundation that creates rotational resistance that behaves closer to a fixed support than to a pinned condition (Isfeld et al., 2018). To identify the influence of rotational stiffness on the effective height and the load-bearing capacity, testing of walls with fixed or partially fixed support conditions at the bottom of the wall is necessary. By measuring the deflections as a function of the wall height, the effective height and thus the k factor can be determined and compared with those provided by codes and standards.

Very little testing on SMW subjected to a combination of axial and lateral out-of-plane loads has been carried out. More tests should be performed as this loading case can occur due to wind loads and earthquakes. Tall walls with slenderness ratios of 30 or larger should be tested with horizontal loads applied in addition to axial loads with different e/t ratios. It is important to spread

the load from the loading frame into the cross-section of the wall so that local failure due to stress concentrations can be excluded (Müller et al., 2017)

In SMW, second-order effects become especially relevant for large axial loads. Therefore, future tests may explore the effects of the axial load when successively increased. In this context, the loading condition for which the failure mechanism changes from strength to stability can be determined.

One of the main reasons for the conservativism on the standards appears to be the underestimated flexural rigidity; therefore, the development of an equation for EI_{eff} that takes account of the slenderness ratio kh/t and the relative eccentricity e/t is needed.

This study presents the results of a PG SMW subject to a constant eccentric vertical load and an increasing out-of-plane pressure. The test setup design was partially based on the ACI-SEAOSC field tests performed in 1980. This is the first of a series of walls that will help to expand the knowledge of the behaviour of SMW and to update the design criteria on the standards for these types of structures.

3 NUMERICAL STUDY OF THE RESPONSE OF REINFORCED SLENDER MASONRY WALLS WITH VARIOUS REINFORCEMENT ARRANGEMENTS[1]

3.1 Introduction

Slender masonry walls are widely used in single-storey buildings, such as gymnasiums and light industrial structures. These walls are susceptible to second-order effects and instability because of their limited flexural stiffness and their tendency to buckle under relatively low axial compression loads. For these reasons, they are restricted by special requirements in the Canadian masonry design standard CSA S304-14. In conventional Reinforced Masonry (RM) construction, steel reinforcement is placed at the centre of the wall. This practice results in inefficient use of reinforcement because it is close to the out-of-plane neutral axis (NA). To overcome this issue, various solutions have emerged for placing the reinforcement farther from the NA.

Near-surface Mounted (NSM) reinforcement is a technique where reinforcement is adhered to the tension side of a structural element to increase strength and stiffness. NSM reinforcement has been extensively used to retrofit structures, cutting groves into walls and placing the reinforcement with epoxy or a cementitious material. Sparling et al. (2018) introduced a new Surface Reinforced (SR) CMU with a pair of channels on the external faces to include NSM reinforcement during the construction of new walls. Enough units were fabricated to build a series of 3.2 m tall by 1.2 m wide panels. Results showed that RM walls with NSM reinforcement using the same steel ratio have higher strength and stiffness than those with a conventional configuration. However, this wall system may come with challenges related to installation times and structural fire safety.

Entz (2019) improved the reinforcement scheme inside the blocks with pre-tied steel cages with specially designed CMUs that are able to slide around the cage to form an in-line boundary element, similar to an embedded concrete column. In this system, the increase in the moment arm of the reinforcement played a major role in reducing Out of Plane (OOP) deflections in loadbearing RM walls. This system enhanced the pre-cracked response, but after cracking the flexural stiffness

[1] Chapter 3 of this thesis has been published, aside from minor formatting edits, as R. Gonzalez, A. Alonso, C. Cruz, and D. Tomlinson, "Numerical Study of the Response of Reinforced Slender Masonry Walls with Various Reinforcement Arrangements" in the proceedings of the 14th Canadian Masonry Symposium in Montreal, Canada.

of the enhanced wall and the conventional wall started to converge. The primary mechanism by which the OOP stiffness is enhanced is through inducing a compressive force in the rebar layer placed in the compression zone. Therefore, this is better suited for high axial load conditions.

In this study, a finite element model was developed using the OpenSEES software framework to perform a parametric analysis to understand the overall behaviour of slender walls under different configurations, and then to analyze and compare an innovative arrangement with other more traditional options. This new configuration of 20 cm thick Partially Grouted (PG) RM walls was proposed placing the steel rebar touching the unit face shell to take advantage of a higher moment arm to resist moments and potentially achieve stiffer SMWs. This solution may present challenges during physical tests, such as a reduced bonding of the rebar to the concrete or early damage to the block face shell; however, the focus of this study was on the potential enhancements that can be achieved. Physical tests of full-scale SMWs are planned as part of this project in the coming months. These tests are intended to expand the knowledge of the behaviour of SMWs and are partially based on the ACI-SEAOSC field tests performed in 1980, which is an often-referenced study for full-scale slender walls.

3.2 Numerical model

A finite element 2D model was developed using a macro-modelling approach in OpenSEES. A wall of 30 non-linear beam-column type elements, with a support at the base restraining movement along the *x* and *y* global axis, and a support at the top restraining movement along the *x* global axis. The number of segments was selected after a sensitivity test to ensure that the results were accurate enough for the purposes of this work; a higher number of segments triggered a variation of less than 0.01% in the results. The first step in the analysis was to apply a static compressive load *P* at the top of the wall at an eccentricity, *e*, both of which are defined by the user. A uniformly distributed load *w* was then applied along the height of the wall until a target midspan deflection was achieved. A schematic drawing of the model is shown in Figure 3.1a. Figure 3.1b shows the simplified section defined in the software, being b = the total width of the wall, w_{gr} = the sum of width of the grouted cells without considering the webs, t = the thickness of the masonry units, and tf = the maximum face shell thickness, not considering block taper. A_{s1} and A_{s2} are the steel areas for each reinforcement layer, and d_1 and d_2 are their depth relative to the compressive face,

respectively. Note that d_2 is d_1 mirrored with respect to the OOP axis for this study. The webs are not modelled because it is assumed that their contribution to the OOP stiffness is negligible.

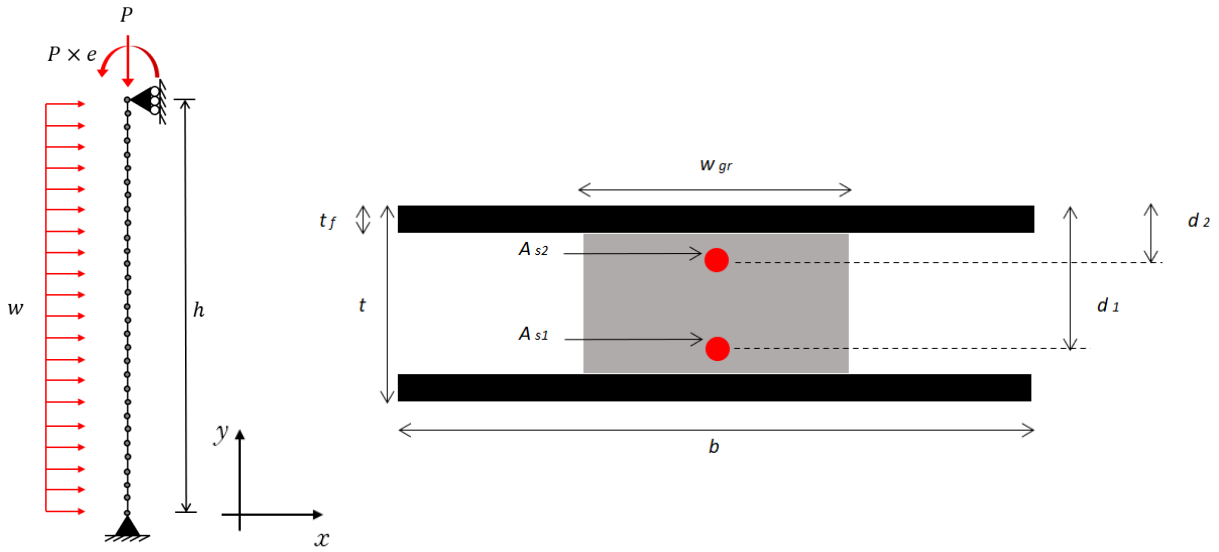

Figure 3.1: (a) Simplified model of the masonry walls (b) Simplified cross-section.

To validate the proposed model, the authors compared model predictions with tests results of two completed studies. In the ACI-SEAOSC study, nine 1220 mm wide and 7500 mm tall concrete masonry panels were built using different CMU thicknesses. Axial compressive load with an eccentricity of half the thickness of each panel plus 76 mm was applied. A gradually increasing lateral pressure was then induced by an airbag on the wall surface until the engineers determined that the tests were unsafe to continue. Figure 3.2 shows the lateral load-displacement curves from both the experimental and the numerical results, where it is seen that the numerical model predicts response, including cracking and post-crack displacements, reasonably well. Peak loads could not be compared since the physical tests were stopped prior to failure because of safety concerns.

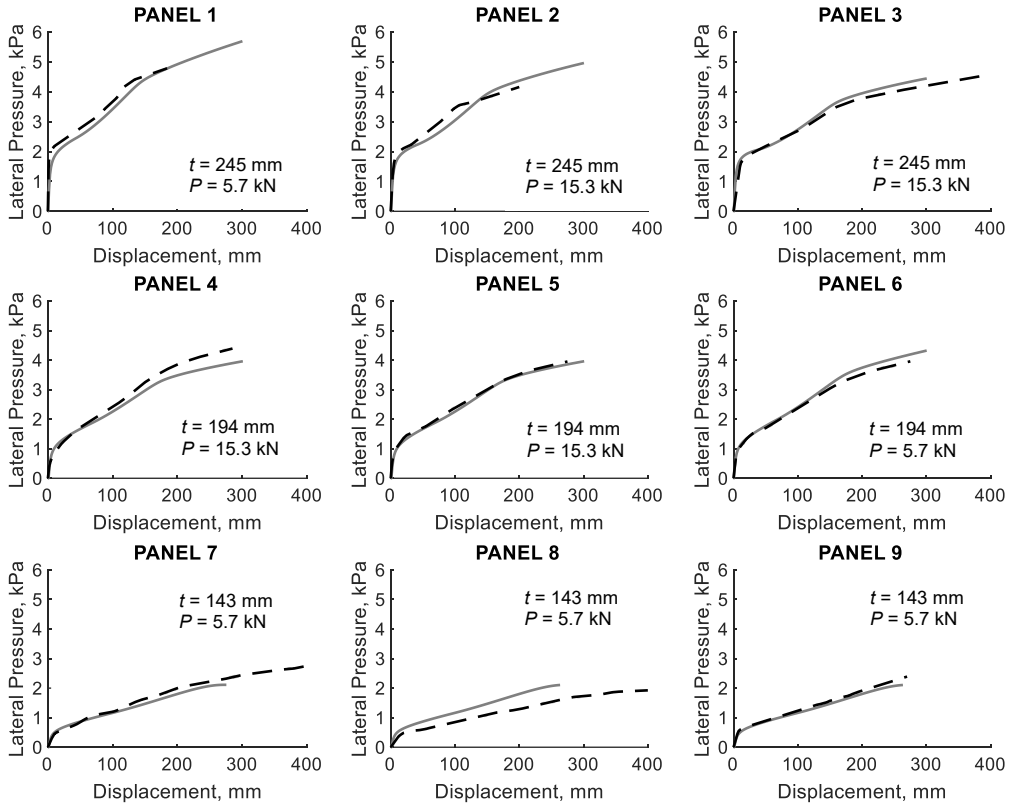

Figure 3.2: Model vs test midspan displacements of walls under loads (ACI-SEAOSC, 1982).

Liu and Hu (2007) applied eccentric compressive load gradually at the top and bottom of twelve 140 × 790 × 2390 mm masonry walls until failure. Figure 3.3 shows midspan load-displacement curves of four panels, both the analytical and experimental results. Only panels with an eccentricity of zero at the bottom are presented here due to the limitations of the model. Eccentricity values at the top are indicated in each graph. Predictions were close to the measured responses in terms of stiffness as well as failure load. Failure loads were predicted within 5% of the tested values.

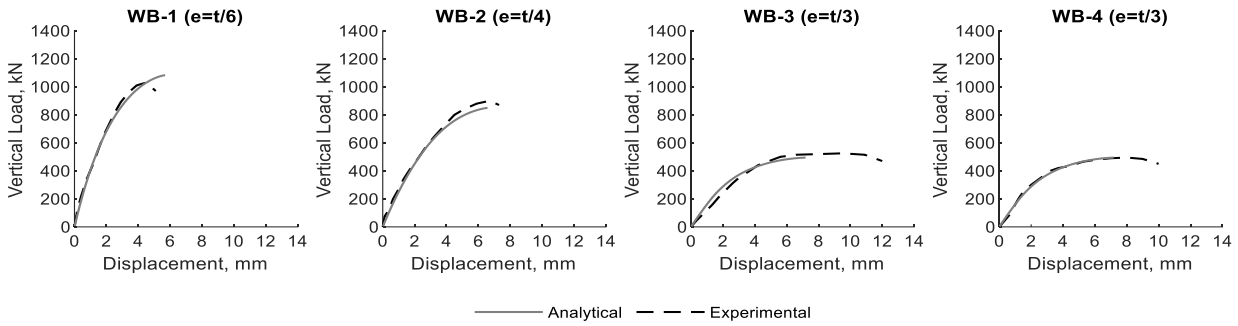

Figure 3.3: Model vs test midspan displacements of walls under loads (Liu and Hu, 2007).

3.3 Parametric study

A series of static non-linear analyses were performed using the computer models to understand the influence of parameters such as the steel reinforcement ratio and depth, masonry strength and the reinforcement yield stress on SMWs. Panels were defined as 8.75 m tall, with a thickness of 190 mm and a width of 1190 mm. These dimensions result in a slenderness ratio (kh/t) of 46, larger than the limit of 30 given by CSA S304-14. A constant load of 15 kN was selected as an appropriate typical axial load. This compressive load is applied at the top of the wall with an eccentricity of 170 mm, based on the eccentricity values used in the ACI-SEAOSC study. Then, a uniform lateral load is applied until a deflection of 300 mm at midspan was achieved. At this displacement, all walls had passed the point where steel reinforcement yielded. Preliminary drawings of the test setup are displayed in Figure 3.4.

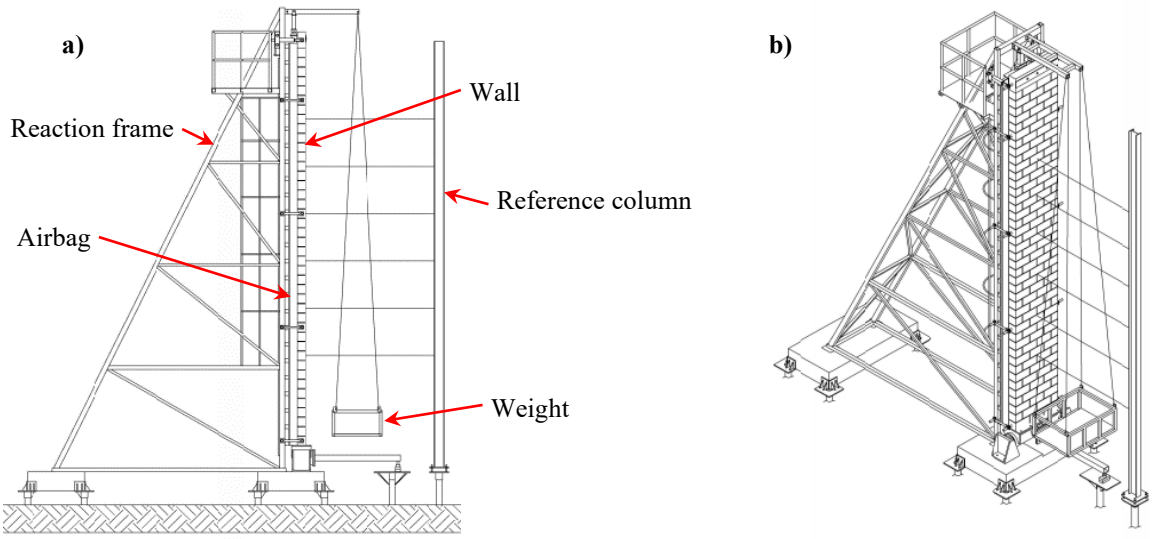

Figure 3.4: 3D Test setup for testing slender masonry walls (a) Lateral view (b) Isometric.

Material properties used in the parametric analyses were based on available experimental data from studies at the University of Alberta (Pettit, 2020), conducted in accordance with Canadian standards. These tests results are representative of materials used in Alberta masonry construction. Masonry prisms had a compressive strength (f'_m) of 16.8 MPa, a tensile strength (f_r) of 0.65 MPa, and a maximum-stress strain of 0.002. Steel reinforcement had a yield stress (f_y) of 533 MPa and an elastic modulus (E_s) of 199 GPa. A volumetric weight of 23.6 kN/m^3 was assumed for self-weight calculations of the wall.

Midspan moment-displacement curves from these analyses are presented in Figure 3.5. Equation (3.1) was used to calculate total moments at midspan, including both primary and second-order moments. Walls were assumed to be single-story with pin-ended conditions as recommended in the Canadian masonry standard.

$$M_{total} = \frac{wh^2}{8} + \frac{Pe}{2} + (P + P_{sw})\Delta \tag{3.1}$$

Where w is the uniformly distributed lateral load due to wind obtained by multiplying wind pressure times the wall width, h is the total height of the wall, P is the axial compression load applied to the top support, e is the eccentricity of the axial load, P_{sw} is the axial load due to self-weight in the centre of the wall, which is half the total self-weight, and Δ is the total deflection.

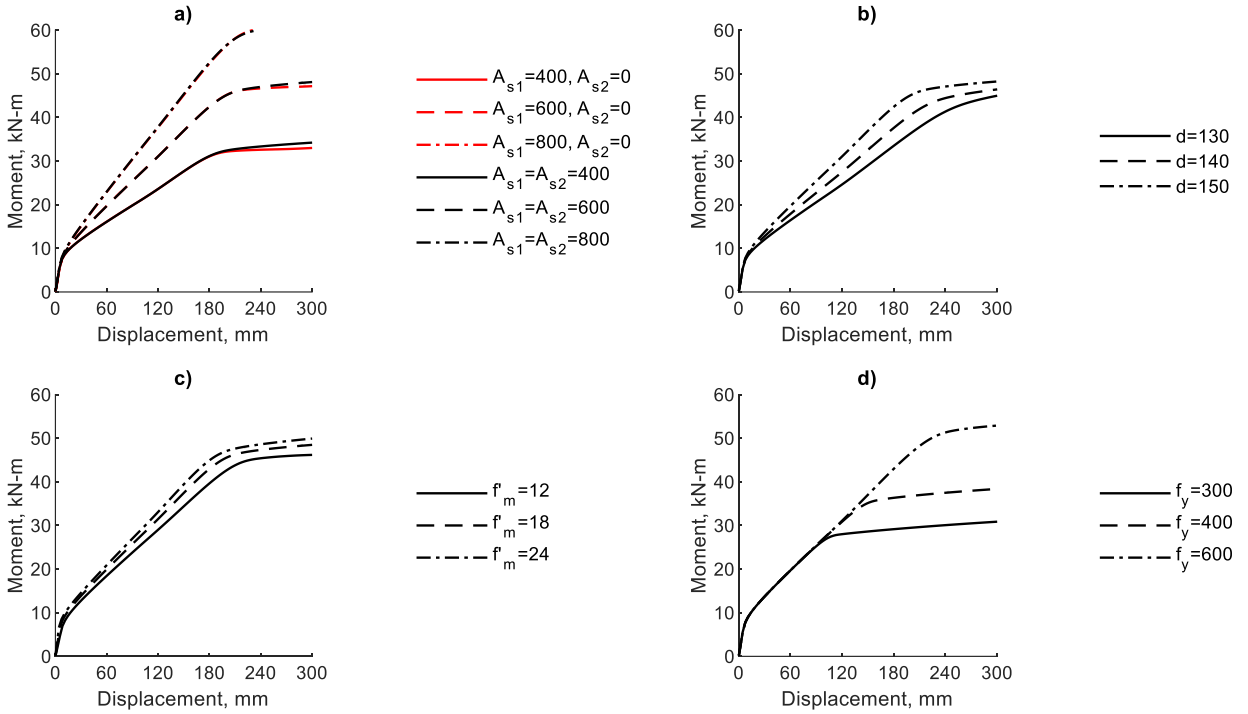

Figure 3.5: Midspan moment-displacement curves from the parametric study (a) Changing reinforcement ratio (b) Changing reinforcement depth (c) Changing masonry compressive strength (d) Changing reinforcement yield strength.

The first parameter evaluated was steel ratio (ρ), defined as the total steel area divided by the gross cross-sectional area. All other properties remain fixed. Figure 3.5a shows responses of walls with different values of ρ. The first three ratios correspond to steel areas of 400, 600 and 800 mm^2 in each layer. The contribution of the compression steel was neglected. The other three, with the same steel area ratios, account for effects that the compression steel may have. The depth of each steel rebar layer was 40 and 150 mm, respectively. Before the cracking moment, at about 7 kNm, there is a negligible difference in the responses of any of the walls. This continues to be true even when other different parameters are varied. After cracking, there is a significant difference in the stiffness of walls with different ρ values, but the effect of the compressive rebar is negligible. According to the model data, this layer of reinforcement was subject to tensile stresses right after cracking occurred. This happens because the out-of-plane neutral axis moves rapidly towards the compression face of the wall. Thus, the formerly compressive steel shifts to be in tension. This suggests that tying rebar to get the benefits of compressive steel will not provide any enhancement for these walls. After reinforcement yields, the moment resistance effectively plateaus for all walls. Results show that increasing steel area greatly improves the response of slender walls.

The second parameter evaluated was the reinforcement depth (d) of both layers. Values of 130, 140 and 150 mm were selected from possible reinforcing arrangements within the wall, using different distances from the rebar edge to the interior face of the masonry face shell. All other parameters remained fixed. In Figure 3.5b, curves show that even a slight increase of *d* results in a higher stiffness after cracking. For instance, at 20 kNm there is a displacement of about 90 mm for a d of 130 mm and about 60 mm for a d of 150 mm, a reduction of 50%. It is important to recall that for slender walls the main goal is to achieve a stiffer section to reduce second-order effects; therefore, increasing d seems like an efficient way of doing so. The yielding moment was close to 45 kNm, followed by a plateau for all three cases.

The third parameter evaluated was the masonry strength (f'_m) using three different values that are likely to be found in practice: 12, 18 and 24 MPa. Figure 3.5c shows very similar curves for the three cases with a small difference in the slope in all stages of the loading. These can be attributed to the change of the elastic modulus of the masonry (E_m) which is a function of f'_m. Since there is not an important enhancement in the response of the walls, there is no reason to increase f'_m.

The fourth parameter evaluated was the yielding stress of the steel rebar (f_y) using values of 300, 400 and 600 MPa. The value of 400 MPa is by far the most common f_y used in construction but it was still interesting to include other possible values in this analysis. The curves in Figure 5d show that changing f_y only causes a larger yielding moment in the wall with the same stiffness before yielding, so there is no motivation to use a higher f_y.

The fifth parameter evaluated was the wall height. Heights of 3250, 6000 and 8750 mm were defined, resulting in slenderness ratios (*kh/t*) of 17, 32 and 46, respectively. This comparison (Figure 3.6) was made to visualize how sensitive these walls are to a change in *d* from 140 to 150 mm. For the 3750 mm wall, taking 20 kNm as reference, the displacement reduction is about 9%. For the 6000 mm wall the reduction is about 18%, and for the 8750 mm wall it is about 28%. These curves serve as an indication that slender walls can benefit from these small changes.

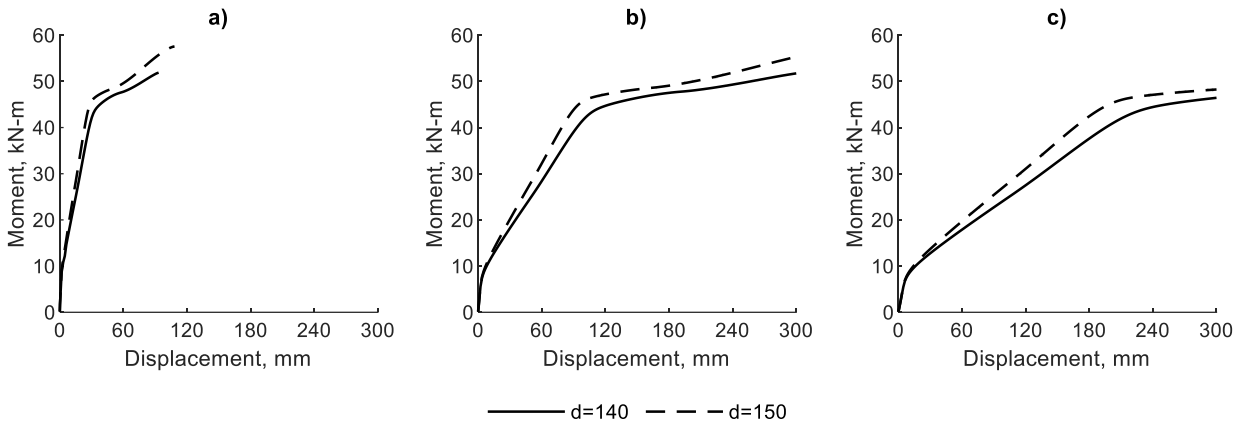

Figure 3.6: Midspan moment-displacement curves changing the height of the walls (a) 3750 mm height (b) 6000 mm height (c) 8750 mm height.

3.4 New Reinforcement Arrangement

From the previous analyses, an arrangement with as much steel area per cell and with the highest reinforcement depth possible is desirable. Increasing ρ and d results in walls with higher out-of-plane stiffnesses. To take advantage of this arrangement the construction process was considered. One limitation is block thickness. Thicker CMUs lead to a stiffer but heavier and more expensive wall. Designing a custom concrete block was an option, but benefits are not sufficient to justify manufacturing costs. Thus, it was decided to work with 20 cm standard units. A second limitation is the hollow cell dimensions and whether cells are grouted or not. Slender walls are sensitive to a change in self-weight, so it was desirable to have the fewest grouted cells that design allows.

The proposal consists of two layers of steel with rebar touching the face shell of the concrete block. This challenges CSA-A371-14 clause 8.2.5.7.1 where the requirement is to have a clear distance of 13 mm between the bar and any masonry surface for coarse grout. By doing this, the reinforcement depth is maximized at the expense of a possible reduction of the bond between the bar and grout. Physical tests will help evaluate if this is a significant effect. The amount of steel in a wall must comply with the minimum area of $0.00125A_g$, where A_g is the gross cross-sectional area, and a maximum of 2% of A_g, according to clauses 10.15.1 and 10.15.2 of CSA-S304-14. Also, the area of vertical reinforcement shall not exceed 6% of the grout space area, as recommended by American standards. Care should be taken with positioning rebar. As discussed before, slender walls are susceptible even a few millimetres change in d. During construction, measures (e.g. stirrups/ties, wire positions) must be used to prevent rebar from shifting from the

desired position along the wall height. Confinement benefits of tight tie spacing are negligible for SMWs with low axial loads, and ties may prevent the vertical reinforcement from reaching the edge of the grouted cell. For this, steel wire positioners may be a better choice knowing that good supervision is needed during construction. Additionally, a proper technique in the application of mortar and the setting of the CMUs is important to minimize mortar fins.

Four 190 × 1190 × 8750 mm PG walls (Figure 3.7) were defined in the model using the same materials and load conditions as described before. Section 1 represents a typical masonry wall having the rebar positioned at the centre. Section 2 has two layers of reinforcement, and the position of the rebar complies with the recommended 13 mm cover from any masonry surface as specified in CSA 304.14. Sections 3 and 4 have two layers of rebar touching the face shell. The difference is that in Section 4, the face shell thickness is slightly reduced from 32 to 28 to gain 4 mm of *d*. Reducing this thickness further may compromise the loadbearing capacity of the masonry.

Using these four sections, three different steel areas were tested in the model. First, a total steel area of 1600 mm^2 was selected to be within the practical limit of 6% in each cell as specified in the standards, meaning up to 854 mm^2 per cell for 190 mm blocks. This exceeds the maximum steel area recommended by clause 10.7.4.6.5 due to ductility requirements. A second value of 800 mm^2 was selected to comply with the maximum steel area for ductility. A third value of 400 mm^2 is selected to represent a more lightly reinforced wall.

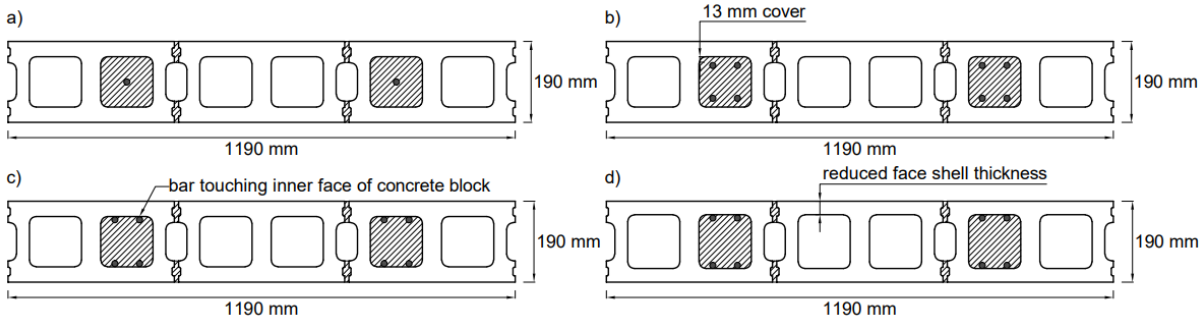

Figure 3.7: Schematic drawings of cross-sections of the analyzed walls (a) Section 1, rebar at the centre (b) Section 2, two layers of reinforcement with 13 mm inner cover (c) Section 3, two layers with no inner cover (d) Section 4, CMU with reduced face shell thickness.

3.5 Expected results

Midspan moment-displacement curves for all the walls are shown in Figure 3.8. In all configurations, no visible change in stiffness is seen before cracking, at about 7 kNm. This portion of the curve is mostly affected by masonry properties since little to no tension is present in the section. For the three groups of walls, sections with a greater reinforcement depth had higher stiffness after cracking, as expected. For all reinforcement ratios, Wall 3 shows a much larger stiffness than Wall 1. For example, taking a reference moment of 15 kNm, displacements are reduced by 35% to 50%. Interestingly Wall 3 is much stiffer than Wall 2 even when the depth increase is only about 13 mm, with displacement reductions of up to 28%. In all cases, Wall 4 response seems close to that of Wall 3, with no significant improvements in either strength or stiffness. It can be assumed that manufacturing a new unit with a reduced thickness is not a feasible way to improve the resistance of these slender walls. Wall 3 has the most promise for evaluation using physical testing.

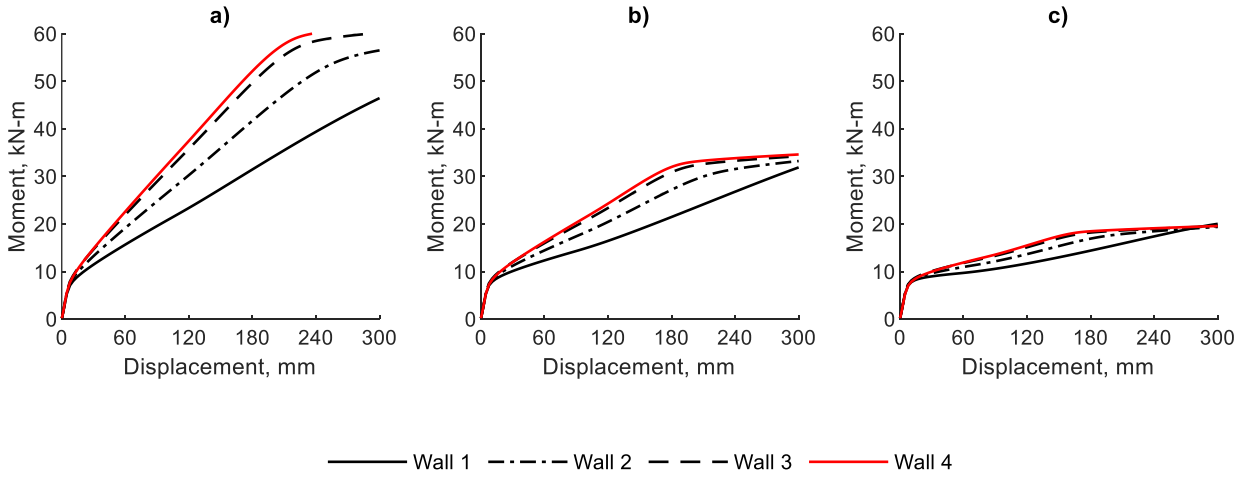

Figure 3.8: Midspan total moment-displacement curves for 190 × 1190 × 8750 mm walls (a) A_s = 1600 mm^2 (b) A_s = 800 mm^2 (c) A_s = 400 mm^2.

Differences between wall responses are more drastic in the group with the highest ρ. This group contains an amount of steel that does not comply with the ductility requirement in S304-14. However, it is seen in these curves that yielding occurs after large deflections, immediately followed by an unstable behaviour. It can be assumed that ductility is not a concern for these slender walls, unlike stability. The third group seems too lightly reinforced for the conditions of the test since it is evident that after cracking, all four sections take large deformations before any

noticeable increase in load resistance takes place. Figure 3.9 shows the same results but with flexural effects decomposed into primary moments and second-order moments at midspan. Because of the slenderness of these walls, second-order effects quickly become important and cause the wall to be unstable at, or even before, the steel has yielded, particularly for the 400 mm^2 walls. These results suggest that the ductility provision should be revised, as it seems to be over-conservative and is preventing designers from using configurations with more steel in the grouted cells.

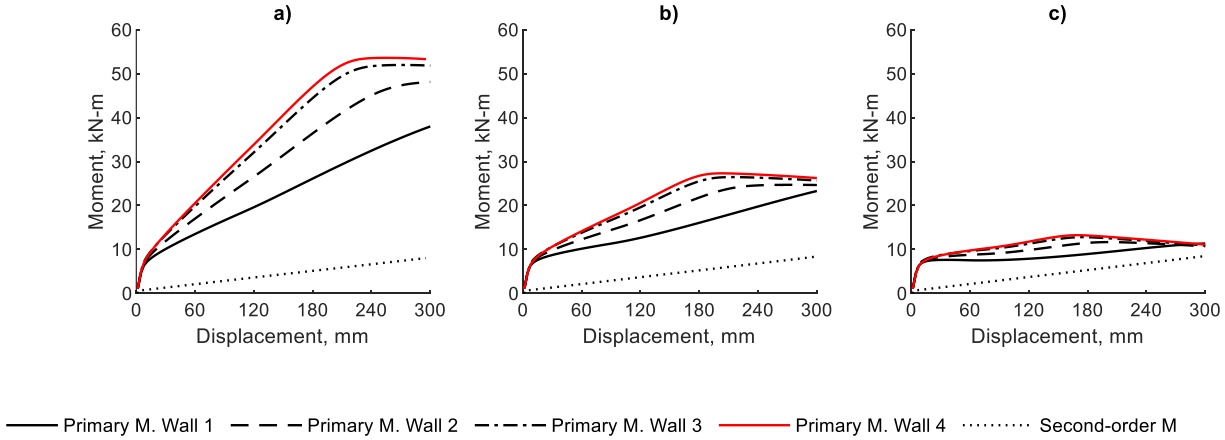

Figure 3.9: Primary and secondary moments at midspan against displacement for 190 × 1190 × 8750 mm walls (a) A_s = 1600 mm^2 (b) A_s = 800 mm^2 (c) A_s = 400 mm^2.

3.6 Chapter Conclusions

The proposed numerical model proved to closely predict the out-of-plane response of SMWs subject to low axial loads and can provide a good understanding of their behaviour under a variety of conditions. This model will be used to design the test setup for the experimental stage and, in the future, to propose new walls to be tested.

A limitation of this model comes from its macro-modelling approach, as it does not predict any local effects like the crushing of the masonry near the supports, spalling of the face shells of blocks or reduced bonding of the reinforcement. These phenomena should be investigated by conducting physical tests.

Section 3.4 presents a section where the steel rebar is touching the internal face of the CMU in an effort to increase the moment arm and reduce second-order effects (Wall 3). This appears to be

a promising solution according to model predictions. Future physical tests should address the feasibility of this solution and investigate the failure mode of these walls.

A more in-depth study must be conducted on the ductility requirements for SMW, found in the CSA-S304-14. Results of this study suggest that slender walls may encounter instability soon after the yielding of the reinforcement, meaning that ductility did not play a major role in the response. Future studies should explore the failure modes of a wider range SMWs.

4 EXPERIMENTAL PROGRAM

4.1 Introduction

As discussed in previous chapters, the primary motivation of this study was to perform an experimental test on a typical slender masonry wall since there is a small number of studies available in the literature for these walls. A 20 cm masonry wall, the most common for single-story buildings in Canada, needs to be at least 5.7 m tall to be considered slender by the design standard S304. Moreover, building walls that challenge this provision and showcase the capabilities of slender walls require ample roof clearance and special testing equipment. Both of these things were not available at the laboratory.

Using experimental tests on scale models could have solved the size problem but included additional challenges. According to Lirola et al. (2017), the requirements for phenomenological similarity between different scales are: geometric, kinematic, dynamic and sometimes thermal similarities. It is virtually impossible to get all similarities simultaneously. For instance, to get equivalent material behaviour in scale models, the material properties such as strength or density should be changed accordingly. Mohammed et al. (2010) investigated the effect of scale on the compressive behaviour of masonry, founding that masonry compressive strength is increased as the scale is reduced. Additionally, the fabrication of specialty masonry units and the deviation from traditional construction procedures in practice made this option not ideal to the author. Therefore, the experimental program consisted of a full-scale concrete masonry wall subject to a combination of eccentric vertical load and a distributed out-of-plane lateral load. The wall was 8.75 m tall with a slenderness ratio (h/t) of 46. The wall was built on a pinned base and supported at the top with a roller. A unique test device was designed and fabricated to make the test possible, and all work was performed in a yard and exposed to the elements.

This chapter presents the properties of the materials used to build the masonry wall, as well as the construction process of the wall. Also, specifics of the test device and the instrumentation for the test are provided. A discussion of the test results is included at the end.

4.2 Material Properties

4.2.1 Mortar

Type S mortar was used during the wall and sample cubes construction. The compressive strength of the mortar was determined by crushing six 50 mm × 50 mm × 50 mm mortar cubes under axial load as specified in CSA A179-14. Test results, shown in Table 4.1, indicated that the average strength at 28 days was 16.8 MPa.

Table 4.1: Test results from mortar cubes.

Specimen	Peak Load, kN	Strength, MPa
1	43	17.3
2	40	16.1
3	42	16.8
4	41	16.5
5	44	17.5
6	42	16.8
Average, MPa		16.8
COV %		2.75

4.2.2 Grout

Course grout with a specified strength of 20 MPa was used to fill the reinforced cells during the wall construction and hollow cells during prism construction. Samples of the grout mix were used to cast four 100 mm × 200 mm cylinders under concentric axial load in accordance with CSA A179. Test results, shown in Table 4.2, indicated a 28-day averaged compressive strength of 24.9 MPa.

Table 4.2: Test results from grout cylinders.

Specimen	Peak Load, kN	Strength, MPa
1	210	26.7
2	189	24.0
3	187	23.7
4	198	25.2
Average (MPa)		24.9
COV (%)		4.72

4.2.3 Masonry

According to CSA S304-14, a minimum of five masonry prisms shall be tested to determine the compressive strength of the masonry assemblage. Five grouted and five ungrouted prisms were built by certified masons while the wall was being constructed. Prisms were five courses tall and one unit wide, laid in a running bond pattern. The combination of both grouted and ungrouted masonry prisms will allow to determine the properties of both and get an averaged strength.

Due to time constraints and lab access, masonry prisms could not be tested at the time of writing. In lieu of the test results for the masonry assemblage, the compressive strength was obtained using the values from Table 4 in S304-14 for units with a specified compressive strength of 15 MPa and calculating the weighted average of the grouted and ungrouted areas in the cross-section. This resulted in a value of 8.5 MPa. Compressive tests of the masonry prisms were unavailable at the time of writing but are planned for the near future, and results will be published when available.

4.2.4 Steel Rebar

The vertical and horizontal steel reinforcement used during the wall construction was Grade 400 15M and 10M bars, respectively. Three 600 mm long bar coupons of each size were tested under tension following the provisions of ASTM A615. Test results, shown in Table 4.3, indicated an average yield strength (fy) of 430 MPa and a modulus of elasticity (E_s) of 198 GPa for the 15M bars, and fy of 452 MPa and E_s of 183 GPa for the 10M bars.

Table 4.3: Test results from steel rebar coupons.

Specimen	Yield Strength, MPa		Elastic Modulus, GPa	
	10M	15M	10M	15M
1	453	-	198	-
2	451	-	192	-
3	454	-	189	-
4	-	426	-	187
5	-	432	-	196
6	-	429	-	197
Average	453	429	192	193
COV %	0.3	0.6	1.9	2.1

4.3 Full-Scale Slender Masonry Wall

4.3.1 Masonry Units

To build a test wall that resembles conventional RM walls built in Western Canada, the materials used were the same as those readily available in the construction industry. The CMU used was the standard 20 cm block, as this is the most common unit found in masonry construction. Actual dimensions are shown in Figure 4.1. The nominal compressive strength for these blocks was 15 MPa. Only standard stretcher units and knot-out lintel units were used to build the wall. For the courses where halves were needed, complete stretcher units were cut to 190 mm instead of using the halves included in the concrete block pallets. The reason for this was to represent a better sample from a larger wall, where most of the units are full-stretcher units.

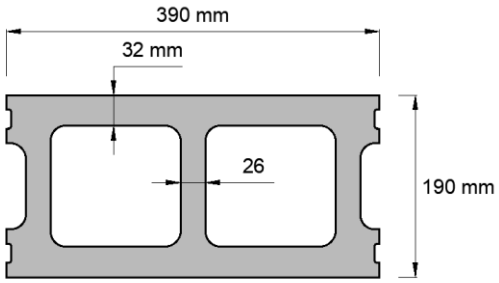

Figure 4.1: Standard CMU used in Western Canada.

4.3.2 Cross-Section

The length of the wall was set as three units, or 1.2 m, to facilitate comparison to other wall tests in the literature. The wall was designed as partially grouted as this is a common configuration found in RM tall walls. Two out of the six cells in the section were filled with course grout, the most commonly used in Western Canada, and the rest were left hollow. Grout was mixed in site

by certified masons from pre-blended bags. The vertical reinforcement used was 1-15M steel bar in each grouted cell, giving a total of two bars in the cross-section. This resulted in a steel area of 400 mm^2 and a reinforcement ratio (ρ) of 0.17%. To secure the vertical reinforcement against displacement during grouting, custom-made steel wire positioners were fabricated on-site and installed at least every 2.4 metres. This complies with the maximum interval of 3 m required by A371 for 15M bars. Cross-section details are shown in Figure 4.2.

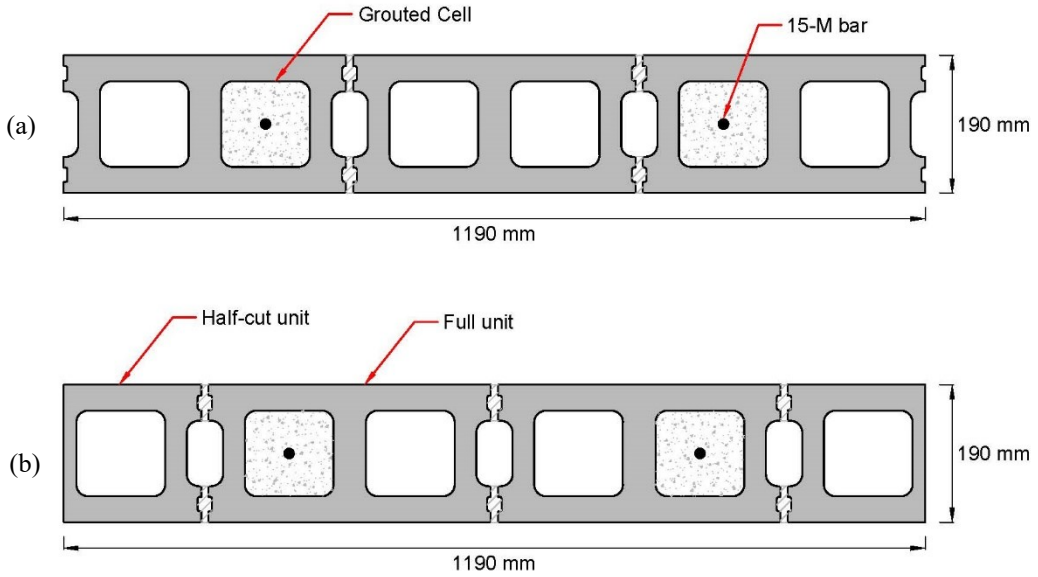

Figure 4.2: Cross-section of test wall (a) Three full-unit course (b) Two full-units and two half-cut units course.

4.3.3 Wall Construction

The height of the wall was 8.75 m, measured from the bottom of the first masonry course to the top of the concrete cap beam, resulting in a slenderness ratio of 46 using actual dimensions. The effective height, measured from the rotational centre of the pinned base to the rotating steel rod at the top, was 8.83 m. This value was used for ongoing calculations as it represents better the length of the pin-pin structure.

The mortar used was a Type S pre-blended mix. The CMUs were laid in a running bond pattern by certified masons, applying mortar to the face shell beds and the most outer webs of the section. Both vertical and horizontal joints were finished with a jointer tool on the front side of the wall. This helped to push the mortar to fill any voids and waterproof the joint, as well as to give a better appearance of the wall. The jointer could not be used on the back of the wall due to the reduced

space between the wall and the airbag. A 1.2 m piece of standard ladder joint reinforcement was installed every two courses or 400 mm. Joint reinforcement is used in walls to resist in-plane shear forces. S304 specifies a maximum spacing of 600 mm for joint reinforcement in non-seismic walls (clause 10.15.1.4) and 400 mm for seismic walls (clause 16.4.5.4). The decision to use a 400 mm spacing considered that future walls of this research program might explore seismic wall configurations, and this first wall will serve as a comparable reference. However, joint reinforcement was not expected to affect the out-of-plane response of this wall. Details of the wall are presented in Figure 4.3.

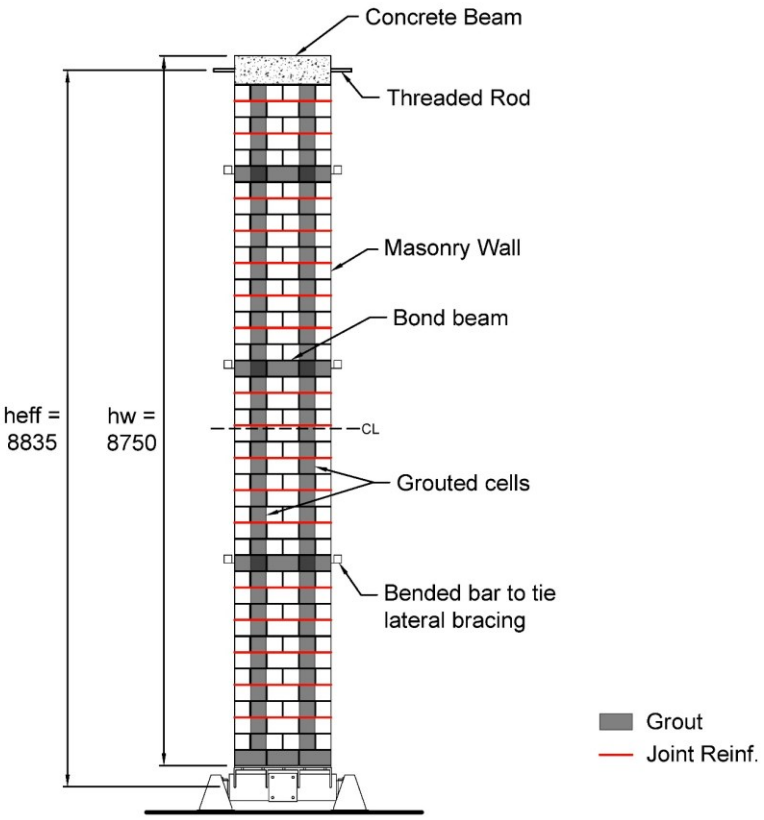

Figure 4.3: Masonry wall specimen details, front view (dimensions in mm).

In practice, these tall walls are located around large clear areas like in warehouses. It is common to lay a few courses over a great length, resulting in large horizontal construction progress in relation to the vertical progress. Using this procedure, masons can work with steel bars with a shorter length that is lighter and easier to handle but result in a larger number of lap-splices. Low-lift grouting was preferred to build this tall masonry wall to reflect this typical construction procedure. However, the central part of the wall was planned as high-lift grouting to avoid having

lap-splices at or near midspan where maximum moments are expected to occur. The construction process is illustrated in Figure 4.4. Cleanouts needed to be provided at the bottom of the high-lift pour segment for every grouted cell, as required by A371; and are presented in Figure 4.5. Cleanout openings allowed to remove any mortar debris accumulated while laying courses on top and to inspect that vertical bar lap splices were correctly tied prior to pouring the grout.

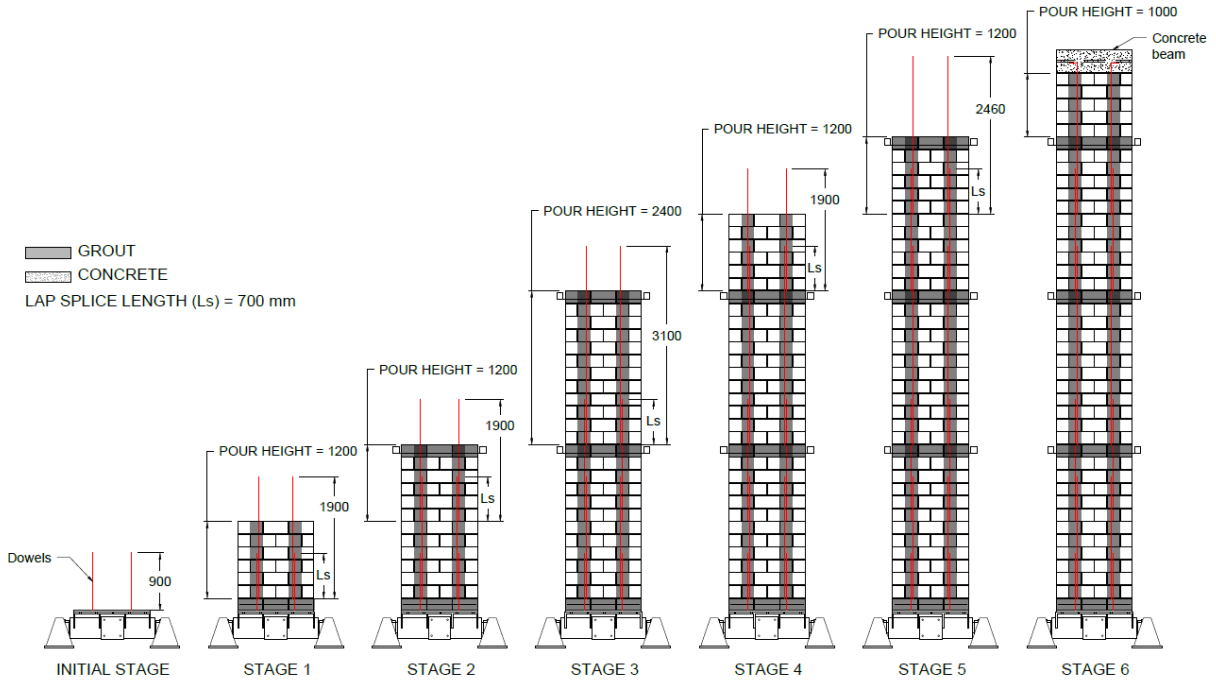

Figure 4.4: Schematic drawing of the construction process for the test wall.

Figure 4.5: Cleanouts as required by A371 (a) Before grouting (b) After grout hardened.

Two 900 mm 15M bars were first welded to the bottom steel plate to serve as dowels coming from the foundation of the wall. The first course was laid using three 20 cm knock-out lintel units on top of the base steel plate, and it was immediately grouted (Figure 4.6(a)). Then, the first set of bars of vertical reinforcement was tied to the dowels using the just grouted bond beam as a base. The lap-splice had a length of 700 mm, which is more than the minimum of 670 mm set by clause 12.4.2 of S304; this length was consistently used for all the other lap-splices on the wall. Six more courses were laid using regular stretcher units resulting in a pour height of 1200 mm. Grout was mixed and poured on the reinforced cells up to the top level of the last laid course. Then, the next set of bars was tied to the protruding 700 mm of the previously embedded bars. Another five regular courses were laid, followed by a bond beam using knock-out lintel units. Figure 4.6(d) shows how knocked-out pieces of block were used to prevent grout from going into the ungrouted cells. A specially bent steel 10M bar was placed in the bond beam, as shown in Figure 4.6(e) to serve as horizontal reinforcement and to tie the wall from the sides to the steel frame. After the two low-lift pouring rounds, eleven regular courses and a bond beam were laid, resulting in a pouring height of 2400 mm. Steel bars were carefully placed and tied to the protruding bars coming from the lower courses. The bottom course of this high-lift pouring stage was prepared with open cleanouts from the cells to be grouted (Figure 4.5). Grout was mixed by the masons and poured into the two grouted cells up to the top level of the bond beam. Following a similar process, two more 1200 mm low-lift pouring sections and a final 1000 mm low-lift pouring section were built. From the final course, the vertical bars protruded approximately 150 mm bent in a 90° standard hook to anchor into the top concrete beam. The wall verticality was continuously checked by the masons as they continued to lay additional courses (Figure 4.6(b)). Figure 4.6(c) shows a wire positioner used to prevent steel reinforcement from deviating from the centre of the cell, as explained in Chapter 4.3.2. Positioners were spaced a maximum of 2.4 meters. Masons were assembling a modular scaffolding system, shown in Figure 4.6(g), during the wall construction to reach the required height.

Figure 4.6: Construction process for the masonry wall (a) Certified mason laying the first course (b) Mason checking the verticality of the wall (c) Use of positioners to secure position of bars (d) Blocking void cells to prevent grout from entering before grouting a bond beam (e) Horizontal reinforcement in bond beam (f) Construction progress view from scaffolding (g) Scaffolding used to build the masonry wall.

The top concrete beam was 350 mm deep, and its main objective was to embed the pieces that allowed the top of the wall to act as a vertical roller support as well as facilitate the application of the vertical load. Four segments of 25 mm PVC pipe and one segment of 50 mm PVC pipe were placed during the construction of the framework, as shown in Figure 4.7(a), to allow an easy installation of four bolts and a steel rod going through the beam. The function of these items will be described in Section 4.4. Longitudinal reinforcement and stirrups on the concrete beam were designed to provide enough strength to resist all loads during the test without compromising the integrity of the wall. The concrete beam after removing the formwork is shown in Figure 4.7(b).

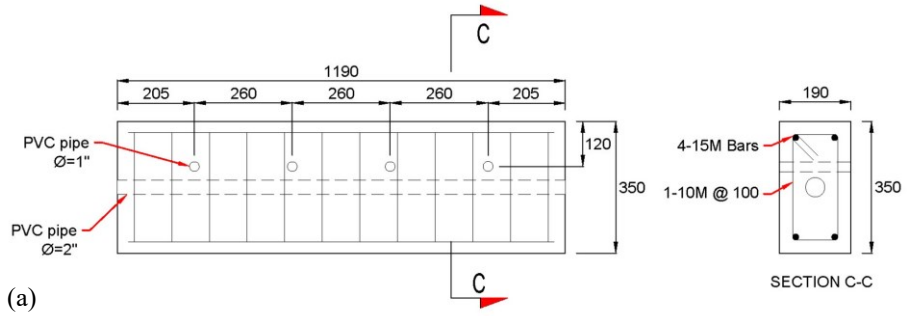

Figure 4.7: Concrete beam at the top of the RM Wall (a) Schematic drawing (b) After removing formwork.

The concrete used to cast the beam was from pre-blended dry mix bags with a specified strength of 27.6 MPa at 28 days. Concrete was mixed in a portable concrete mixer and poured into the beam using plastic buckets. After two days of curing, the framework was removed.

During the construction of the masonry wall, three points of the wall were braced to prevent premature damage or displacements before the mortar and grout hardened. This is a common practice for tall walls since they are not designed to stand as cantilever structures during construction. Each bracing consisted of two 89 × 89 mm wood joists, one on each face of the wall, secured to the steel frame by a couple of 19 mm threaded rods. Bracings were removed immediately before the test and replaced by loose chains that allowed the wall to deform to an extended limit of approximately twice the expected displacement during the test at each point to prevent a sudden collapse in case of loss of stability. Both systems are shown in Figure 4.8.

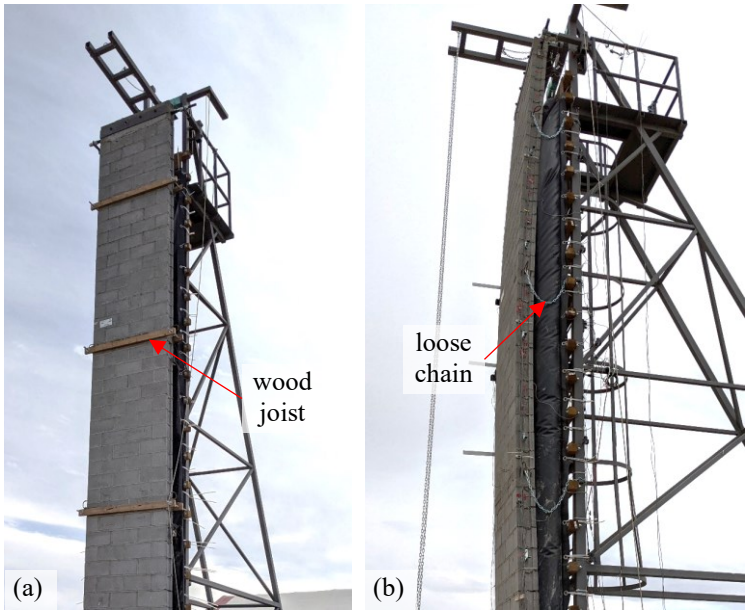

Figure 4.8: Lateral bracing of the wall specimen (a) Temporary wood joists bolted to the frame (b) Loose chains to restrain excessive displacement on the wall during test.

The construction process lasted six days, from the beginning of the first course to the removal of the framework for the top concrete beam. Reasonable efforts were made to test the wall at 28 days from the last day of its construction, but schedule constraints made the test to be delayed to the 35th day.

4.4 Test Setup

4.4.1 Foundation

For the foundation of the test setup, the decision was to use two concrete precast slabs supported by screw piles. Screw piles are constructed of helical plates welded to a hollow steel pipe and are

rapidly installed without additional preparation of the soil (Figure 4.8). This system provides immediate loadbearing capacity after installation and is resistant to frost heave.

Foundation screw piles needed to resist a factored compressive force of 50 kN in soil conditions that vary from stiff clay to compact sand, according to the tests reported by HongBo Xu (2018). HongBo Xu (2018) presents uplift and compression load tests on 96 screw piles, all of them in Alberta. Based on the dimensions of the piles in the report, it was proposed to have two-helix piles with a shaft diameter of 114.3 mm, helix diameter of 406 mm and a total length of 4500 mm. The design was sent to the piling company and then approved. There was no geotechnical study for the specific site conditions of this project location.

Piles were distributed on the site to serve as supports for the concrete slabs, placing one pile for each slab corner. Once the piles were screwed into the ground, the protruding pile shafts were marked with the help of a laser level and cut. Pile caps with bearing steel plates were welded on top of the shafts by a certified welder to provide a flat levelled surface to receive the slabs (Figure 4.9).

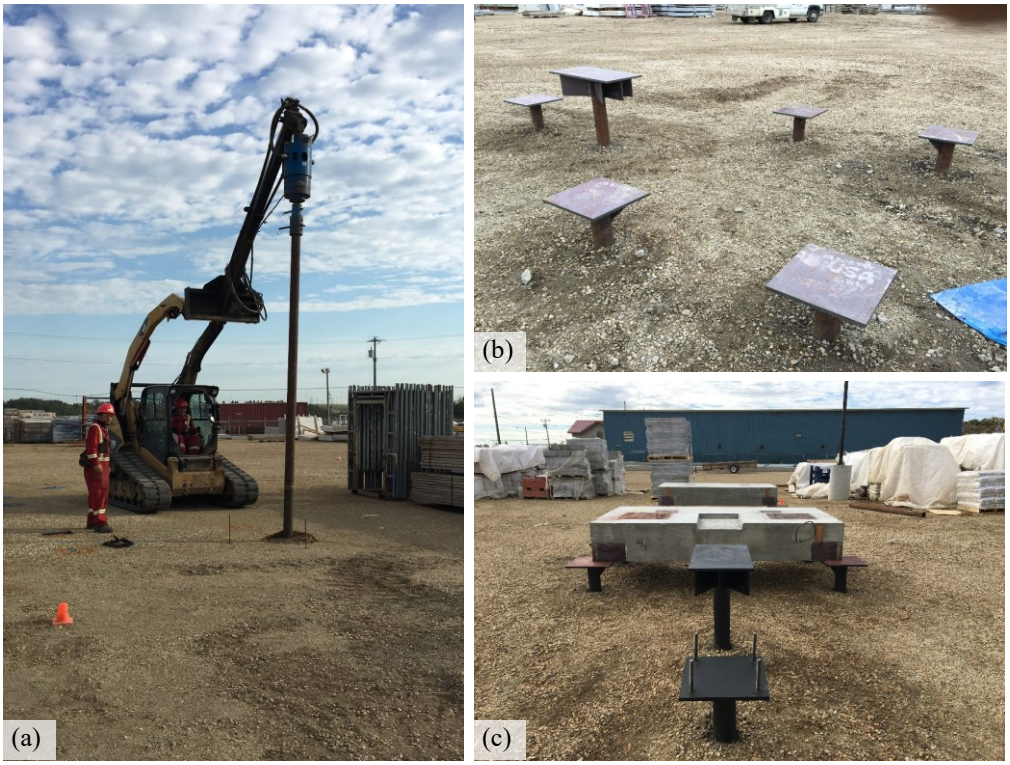

Figure 4.9: Foundation system for the test setup (a) Installation of screw piles (b) Pile caps installed and aligned (c) Precast slabs placed on top of the pile caps.

Two 400 mm thick precast concrete slabs were placed on top of the pile caps. These slabs were built with embedded steel plates on the bottom of each corner to be welded to the pile caps bearing plates and on the top surface to be welded to the main steel frame. Dimensions of the slabs and details on the reinforcement and embedded plates are presented in Figure 4.10.

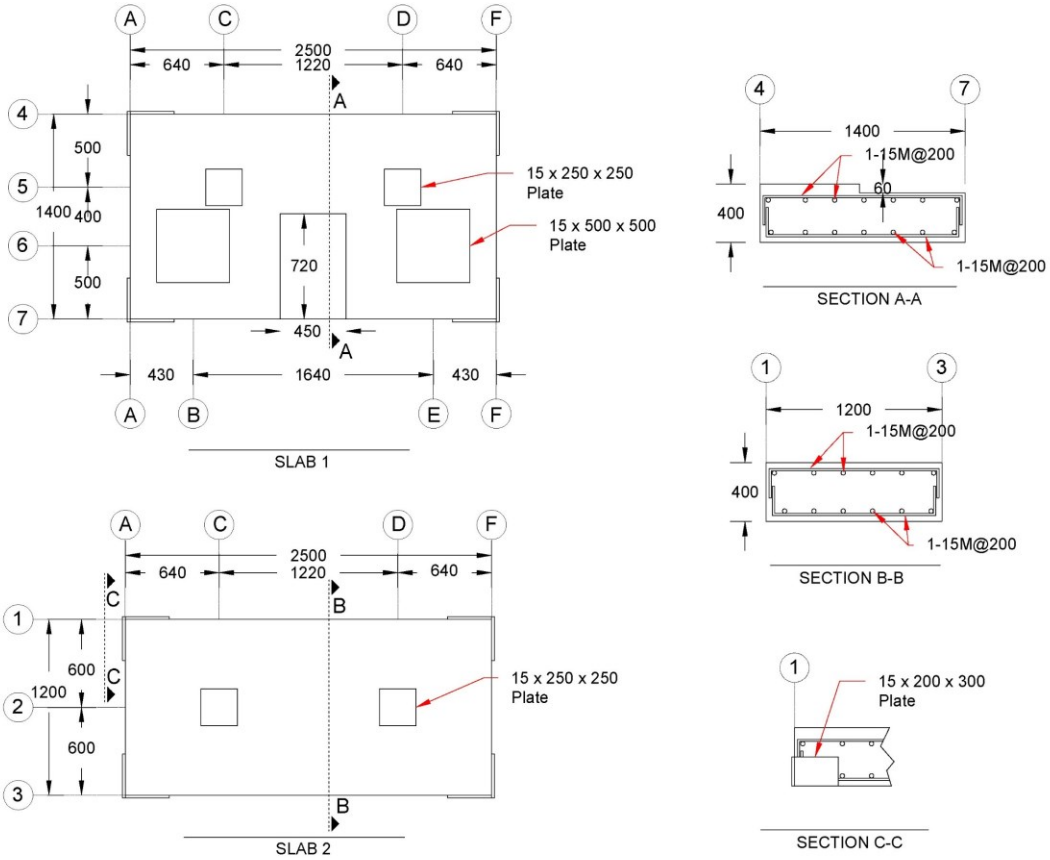

Figure 4.10: Detailed drawing of precast concrete slabs.

4.4.2 Steel Frame

To support the lateral reaction of the airbag pushing the wall, a steel-truss structure was fabricated and installed on top of the concrete slabs. The steel frame was 10 m tall, 5 m long, and 1.2 m wide, with more details provided in Figure 4.11. This structure was designed considering a maximum vertical load of 15 kN applied on top of the wall, and a maximum pressure of 10 kPa applied on the surface of the masonry wall, with a safety factor of 3. Therefore, the factored vertical load was equal to 45 kN, and the factored out-of-plane load was equal to 30 kPa. These loads were obtained considering expected future tests on this same apparatus. During the design, a major concern was to have sufficient stiffness in the steel frame to prevent distorted readings from the displacement

sensors because the measurements of wall displacement were relative to the steel structure. The geometry of the truss and thickness of all elements were designed with this objective in mind. According to the computer model of the structure, a maximum displacement of 1.5 mm occurred at the top of the truss when factored vertical and airbag loads were applied, a number considered sufficiently low by the author.

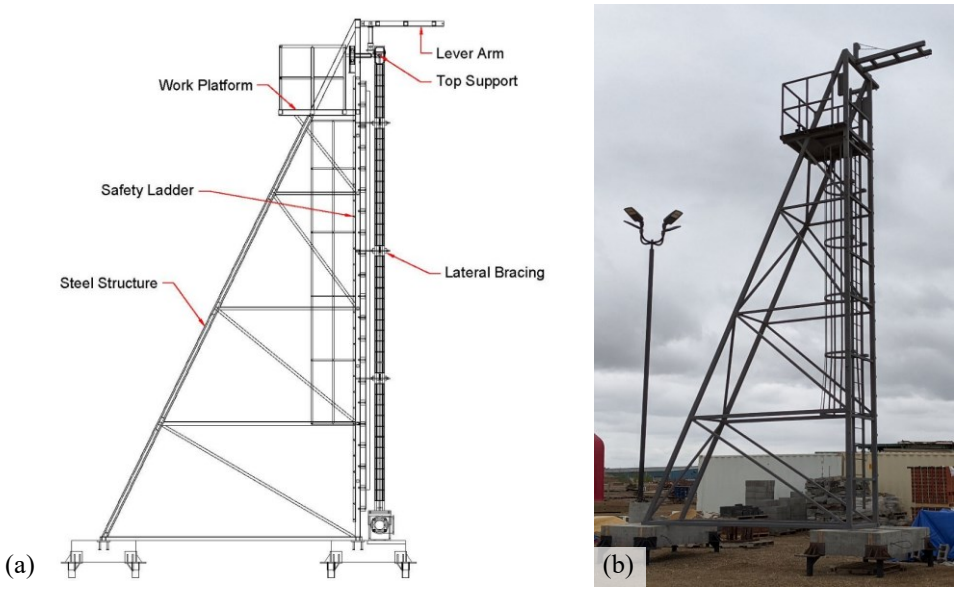

Figure 4.11: Steel structure to test tall masonry walls (a) CAD drawing (b) Photo

The frame included several fixtures to comply with the test's requirements. A series of threaded inserts were positioned on the columns facing the wall to receive the threaded rods used for the lateral bracing during construction and to secure the chains used for bracing during the test. A safety ladder was included inside the steel structure to climb to a platform that allowed to reach the upper portion of the wall and the top support (Figure 4.12a and 4.12b). From the platform, there was access to a pulley fixed to a protruding arm of the structure that was used to lift tools or materials required, as it was unsafe to carry these items while climbing the ladder. Another pulley was installed to lift the lever arm to the desired angle, as this was required during the installation of fixtures and sensors on top of the wall (Figure 4.12c). The top support, also part of the steel frame structure, is shown in detail in the following section.

Figure 4.12: Some fixtures included in the test device (a) Safety ladder installed to reach the work platform (b) Work platform close-up (c) Pulley to lift the lever arm.

After completing the design of the steel structure, the fabrication process started at the manufacturer's workshop. The truss was erected in site and welded to the embedded plates in the concrete slabs by the manufacturer's crew.

4.4.3 Vertical Load System

To transfer an eccentric vertical load on top of the masonry wall, a couple of HSS beams were bolted at the top of the main frame, restraining movement but allowing for rotation. Each beam included a segment of bolted HSS column that would rest on the wall to apply load. These beams were used as lever arms, having a connector at the farthest end from the wall to hang a 6.3 mm chain. The two chains were connected on the lower end to a plastic water tank that was suspended 1.20 m above the ground; enough distance to prevent it from touching anything else during the test. The tank could be filled or emptied using a hose connected to an electric transfer pump. Photos of the lever arm and the hanging water tank are shown in Figure 4.13.

Figure 4.13: Vertical load application system (a) Chains connected to the lever arm on top of the structure (b) Suspended water tank used to apply vertical loads.

To receive the load from the HSS column and transfer it to the wall, a 1200 mm long 150x150x9.5 mm steel angle was bolted to the top concrete beam, as presented in Figure 4.13. Five 19 mm bolts passed through the angle and the concrete beam, to be tied with nuts at the other end. Segments of PVC pipe were used when casting the concrete beam (Figure 4.7) to allow the bolts to pass through the element and to make it possible to recover the bolts after the test. The angle was stiffened with a series of 9.5 mm thick plates welded below the bearing surface to stiffen the element and ensure an even distribution of the loads applied from the small HSS columns.

Figure 4.14: Steel angle connected to the top concrete beam to transmit eccentric vertical loads.

Between each HSS column and the steel angle, two steel blocks with a half-cylinder cut each one was placed and bolted. A cylindric steel piece was placed between these blocks to create a device that locked the columns in position but allowed free rotation of the angle, as shown in Figure 4.15.

Figure 4.15: Special pin connector at the top of the wall.

4.4.4 Top Support

The boundary conditions at the top support of the wall were defined as locked horizontal displacement with free vertical displacement and free rotation. To simulate these conditions, a 1 ½" steel rod was introduced in the concrete beam through the previously embedded PVC pipe. The rod was long enough to protrude from each side of the wall. Each end of the steel rod was threaded to secure it to a steel piece coming from the main steel frame. This piece, one on each side, consisted of a plate with a hole welded to a tee-shaped fixture, and the rod was passed through the hole before a nut was installed to secure the rod from lateral displacement. Each tee-shaped fixture had a couple of bearing wheels that ran inside a rail installed on the main frame. This system permitted the pieces to move up and down but not in a perpendicular direction to the surface of the wall. Details are presented in Figure 4.16.

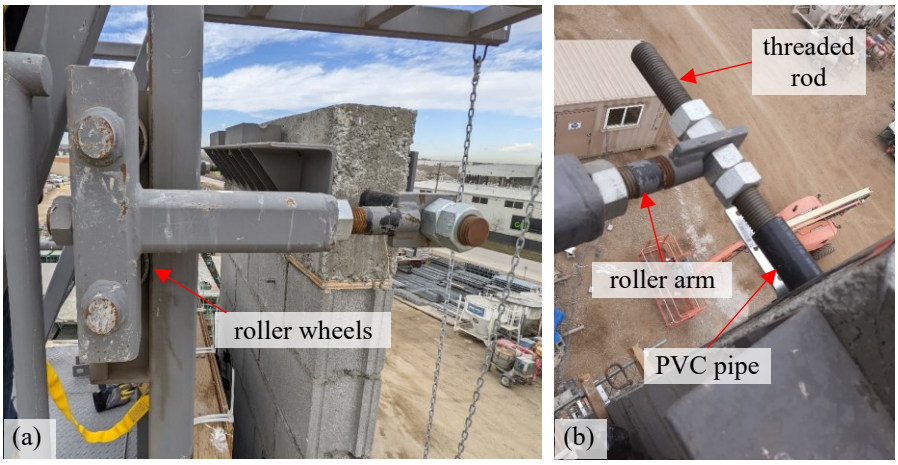

Figure 4.16: Top support system (a) Roller installed on each side of the structure (b) Threaded rod protruding from each side of the concrete beam.

4.4.5 Rotational Base

A rotational base, used previously by Entz (2017) and specially fabricated to behave as a pin support for 3-unit length walls, was installed on top of a concrete slab. This base had a bearing plate attached to a rotating cylinder supported by a couple of steel plates. The base was lifted with a forklift and dropped in the slab while a series of previously welded threaded rods were inserted in the holes found on the base plates. Then, nuts were tightened to secure the base in position and prevent movement. Details of the rotational base installation are provided in Figure 4.17.

Figure 4.17: Rotational base installation (a) Threaded rods welded to the plates on the slabs (b) Device lifted by a crane to install on top of slab.

After installing the base, it was locked with four pedestals especially fabricated to safely prevent any rotation of the pin base during the construction of the wall and before the test procedure. These pedestals were adjustable to allow an easy installation and removal when needed. For each wall to

be tested on the tall wall testing device, a set of steel bars had to be welded to the base to act as dowels from the foundation. To make this without damaging the rotational base, a separate steel plate of the same size as the one on top of the base was prepared with the dowels and bolted to the plate in the base. Figure 4.18 presents the plate with dowels and installed on the rotational base, prior to construction of the wall.

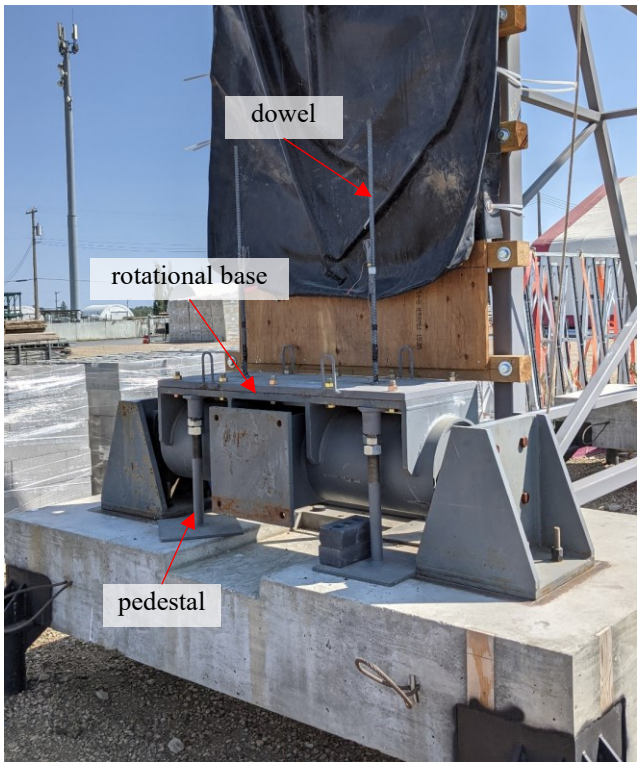

Figure 4.18: Rotational base, plate and dowels installed.

4.4.6 Airbag

Application of out-of-plane loads was performed with an airbag pushing between the steel frame and the wall surface. The airbag was of special fabrication for the use of these tests, designed to inflate like a parabola similar to the deflection expected on the masonry walls. The purpose of this was to reduce the risk of losing contact at the centre of the wall, as reported by the SEASC task force (1982), when the wall started to follow a parabolic-shaped out-of-plane displacement.

To support the airbag and secure it on its place, a wooden structure was mounted on the front surface of the steel frame. First, 89 × 89 mm treated wood joists spaced 400 mm centre-to-centre were bolted to the columns of the frame using 19 mm bolts, nuts and washers. On top of them, 19

mm treated plywood sheets were screwed, providing an even surface from the bottom to the top of the structure, as shown in Figure 4.19.

Figure 4.19: Wood backing system to support airbag (a) Installation of wood joists (b) Installation of plywood sheets.

The airbag was lifted using pulleys installed on the top of the steel structure and ropes. Once the airbag was at the desired height, previously marked on a plywood sheet, it was tied from the flaps to the HSS columns of the steel truss using heavy-duty cable ties. The wood joists were closely spaced and helped to lock these ties from any vertical displacement. Photos of the airbag before and after installation are presented in Figure 4.20.

Figure 4.20: Airbag (a) Before installing (b) Installed and fully inflated.

4.4.7 Inflating System

A 373 W air compressor was installed next to the testing device to inflate and deflate the airbag during testing. The compressor was mounted on a wheeled cart to facilitate movement from the storage to the work area. The compressor had a lever to switch between pressure and vacuum operation. A hose ran from the compressor to the bottom of the airbag, where a ball valve and a pressure gauge were already installed. The valve allowed the system to maintain pressure inside the airbag if the compressor had to be turned off. Photos of these components are shown in Figure 4.21.

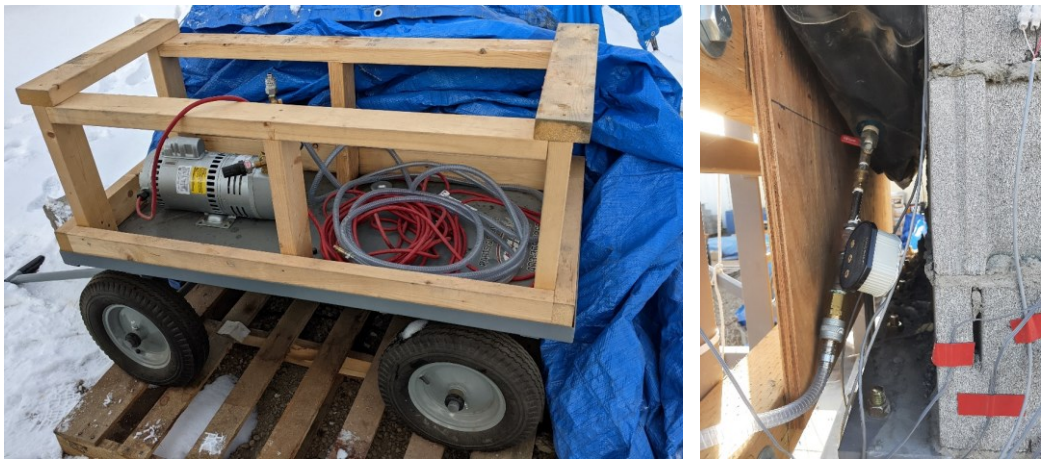

Figure 4.21: Inflating system for wall test (a) Compressor and hose installed on a wheeled cart (b) Valve and connectors plugged into the airbag.

4.5 Instrumentation

The objective of the instrumentation was to capture the overall response of the wall subject to axial and out-of-plane loads, recording both the loads and the deflections. Additionally, strain gauges were installed in various locations to get the performance of the materials in the wall cross-section. The list of sensors used during the test is presented in Table 4.4. These instruments were distributed on the supports and on the wall, as shown in Figure 4.22.

Table 4.4: List of sensors used to test the masonry wall.

Sensor	Quantity	Measurement
Load Cell	2	Vertical load
Pressure Gauge	1	Pressure inside airbag
String Potentiometer	10	Out-of-plane displacements
Inclinometer	2	Rotation at supports
Strain gauge (6 mm)	16	Strains in rebar
Strain gauge (60 mm)	16	Strains in concrete block

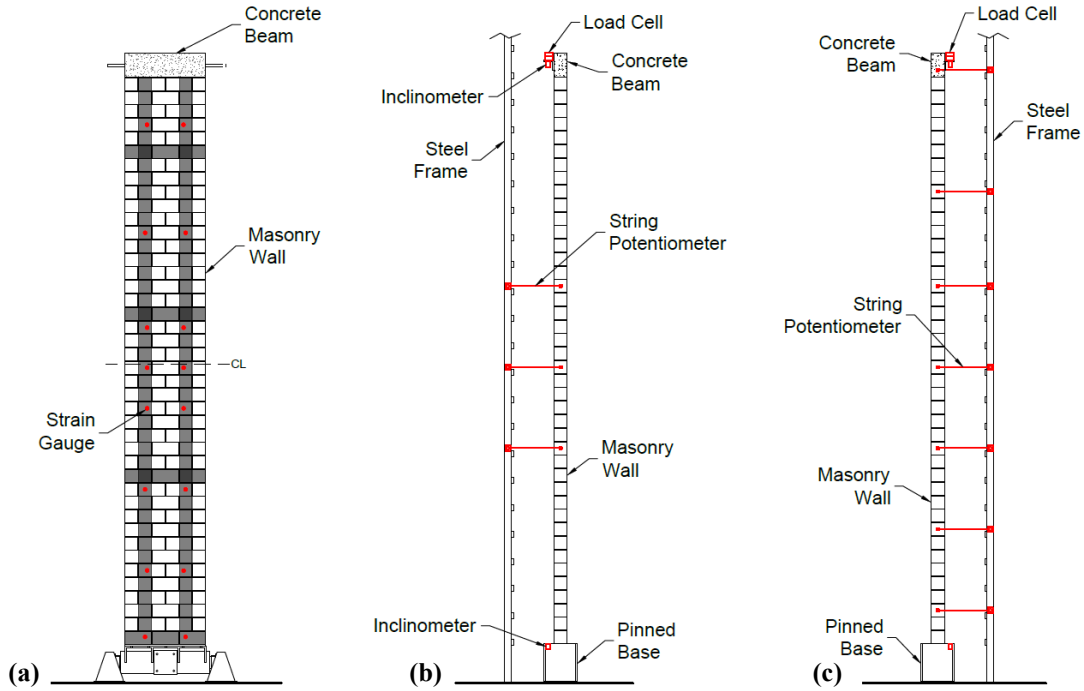

Figure 4.22: Location of sensors installed on the test wall: (a) Front view, (b) Left View, (c) Right view.

Two compression-only load cells were installed in a dedicated slot between the lever arm and the columns that transferred vertical loads to the wall (Figure 4.23a) to monitor the total vertical load applied. The pressure applied by the airbag to the wall surface was monitored by a digital pressure

gauge connected close to the air entrance of the airbag, as presented in Figure 4.23b. Shortly before the test, it was observed that having the compressor functioning affected the readings of the pressure gauge. This meant that the compressor had to be turned off at defined time intervals during the test to get accurate readings. Details on how this affected the test are presented in section 4.7.1.

Figure 4.23: Instruments used to read loads applied (a) Load cells (b) Pressure gauge.

Out-of-plane displacements were captured by ten string potentiometers (Figure 4.24a) attached to the main frame at the locations previously indicated in Figure 4.22 using magnetic holders. Seven of these potentiometers were distributed on the right side of the wall to capture the overall deflected profile; the rest were placed at repeated locations but on the left side, to corroborate readings and detect any torsional behaviour on the wall. Two inclinometers (Figure 4.24b), one on each end support of the wall, were also mounted with magnetic holders to record the rotation during the test.

Figure 4.24: Instruments used to read displacements (a) String potentiometers (b) Inclinometers.

Additionally, 32 strain gauges were installed both on reinforcement and blocks to assess the response of both materials in the cross-section of the masonry wall. The strains in the steel reinforcement were measured by fitting eight pairs of 6 mm, 120 Ω strain gauges at different heights. Every pair was located at the same course, with one sensor on each grouted cell. One pair was located at midspan, and the rest were spread on the wall. At the same level of the rebar strain gauges, two 60 mm, 120 Ω gauges were placed on the surface of the compressive face shell of concrete blocks. This distribution, previously shown in Figure 4.22, allowed to capture the strain profile of the cross-section from the right and left grouted cells at different heights. Both types of strain gauges already installed are shown in Figure 4.25.

Figure 4.25: Strain gauges installation (a) On rebar and completely coated (b) Installed with adhesive on concrete block.

4.6 Methodology

First, vertical load was applied by pumping water into the plastic water tank previously hung from the lever arm. The tank was filled until the reading of the load cells summed a total of 15 kN. At that point, the pump was shut off, and the valve closed to maintain a constant weight applied during the test. Then, out-of-plane loads were applied by turning on the air compressor and inflating the airbag. Once the airbag made contact with the wall, it started to push against the wall surface. The compressor continued to inflate the airbag until the desired midspan displacement was achieved. The airbag was then deflated using the compressor vacuuming feature until the pressure reading was zero and the wall stabilized. This was done for six cycles with different base conditions and goal midspan displacements, as presented in Table 4.5.

Table 4.5: Cycles performed for the wall test.

Cycle	Base Condition	Goal Midspan Displacement, mm	Goal Midspan Displacement, *h/t*
1	Pinned	25	1/350
2	Pinned	25	1/350
3	Fixed	N.A.	N.A.
4	Pinned	48	1/180
5	Pinned	48	1/180
6	Pinned	200	1/44

All cycles, except for cycle 3, were performed with the wall base allowed to rotate freely (pinned-base). Cycles 1 and 2 had a goal displacement of 25 mm at midspan, as it was predicted that the wall would remain linear-elastic at this stage according to numerical models. Cycle 3 was performed with the rotational base locked (fixed-base) using adjustable steel pedestals (Figure 4.18). For this cycle, the goal was to reach a similar pressure to that of the pinned-base cycles 1 and 2. If the goal was displacement, there could be damage in the wall as it would require a higher load to get to 25 mm. The goal pressure would be determined during the test and is presented in detail in section 4.8. Cycles 4 and 5 had a goal midspan displacement of 48 mm or *h*/180, which is the maximum allowed displacement under service loads required by the Canadian masonry standard. Cycle 6 had a goal midspan displacement of 200 mm, as this was previously estimated to be close to the yielding of the steel bars. The wall was not pushed to complete material or stability failure due to safety concerns.

4.7 Pinned-Base Cycles

4.7.1 Results and Discussion

The midspan load-displacement curve of the concrete masonry wall is shown in Figure 4.26. This graph includes the response of the wall under cycles 1, 2, 4, 5 and 6. Since cycle 3 was performed under a fixed-base condition, its results and a comparison with the pinned-base condition cycle are presented in section 4.8. Displacements presented in this section were obtained from sensors mounted on the right side of the wall; it was verified that readings on the left side match by more than 95% to those on the right. The pressure was captured by the pressure gauge, but because of the configuration of the air feed, the compressor had to be stopped at time intervals of about ten seconds to prevent the airflow from affecting the readings.

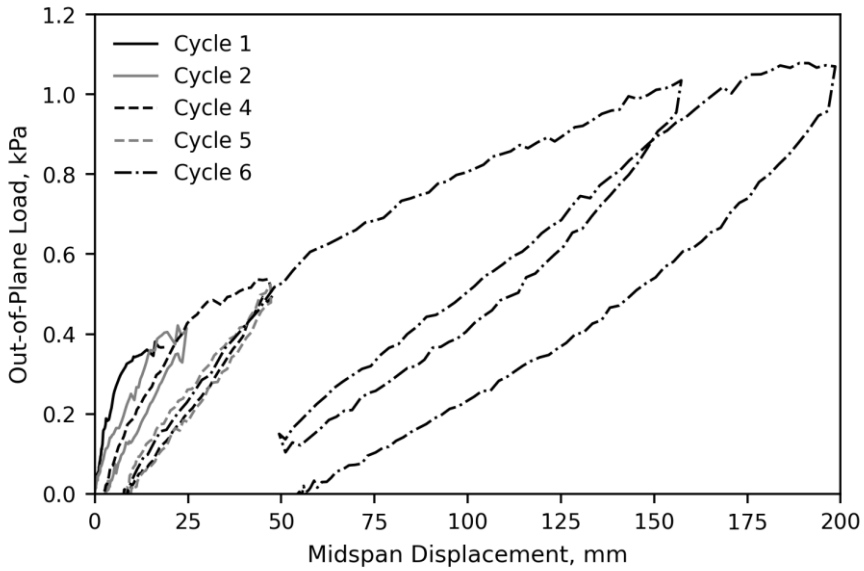

Figure 4.26: Midspan load-displacement curve for the pinned-base condition test.

Cycle 1 was not completed because it was noticed during loading that the airbag was coming out of both sides of the wall and made contact with a string potentiometer cable which affected the readings. However, it was observed during cycle 1 that the wall stiffness started to decrease before the test stopped. This is attributed to the development of cracks and is consistent with the initial behaviour of cycle 2 where the initial stiffness was lower than cycle 1. Some string potentiometers were relocated to prevent contact between the airbag and the cables and avoid issues seen in cycle 1. Cycle 2 starts with zero initial displacement due to data lacking from the residual displacement after the end of cycle 1. Since the wall incurred some damage (cracking) during the first cycle, it is possible that there were a few millimetres of residual displacement not shown in Figure 4.26. Cycles 4 and 5 pushed the wall to a midspan displacement equal to the serviceability limit of $h/180$ required by S304-14 (48 mm), and the wall was unloaded by gradually deflating the airbag until sensors showed that the wall displacements stopped to reduce for both cases. In the 6th and final cycle, the wall was pushed to a midspan displacement of 200 mm. This cycle was interrupted at around 150 mm of midspan displacement because displacements were incrementing faster than expected, and the interval of ten seconds to turn off the compressor seemed too large to capture the wall response. The wall was unloaded to a midspan displacement of 48 mm, the peak displacement of the last complete cycle, and then the loading resumed with new intervals of two seconds to turn off the compressor. This situation created part of an additional cycle, but it is

reported in the rest of the document as part of cycle 6. It was observed that the out-of-plane stiffness reduced near the end of the last cycle, followed by a plateau between 180 and 200 mm. This indicates that steel reinforcement started to yield, as will be discussed in the following paragraphs. Figure 4.27 shows the state of the wall at the peak load of cycle 6, at 200 mm of midspan displacement.

Figure 4.27: Test wall at peak load of cycle 6, taken from left and right sides of the setup.

Figure 4.28 shows the displacement profile of the wall at the peak load of each cycle. Note that the effective height shown in Figure 4.28 is the measured pin-to-pin distance; a line showing the location of the wall base is included for reference. The displacement profiles of all cycles showed a response that was expected from a pin-pin condition and a centred load, with a single curvature and the largest displacement at midspan.

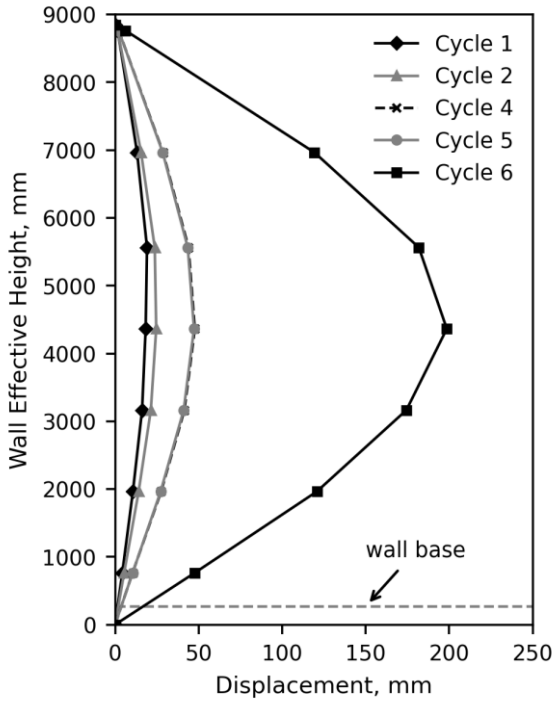

Figure 4.28: Displacement profile of the wall at the peak load of every cycle.

The rotations measured from inclinometers at both ends of the wall during the test are shown in Figure 4.29. Both top and bottom supports had virtually the same rotation, suggesting that supports allowed free rotations as desired, getting close to 4° at the peak load of the last cycle.

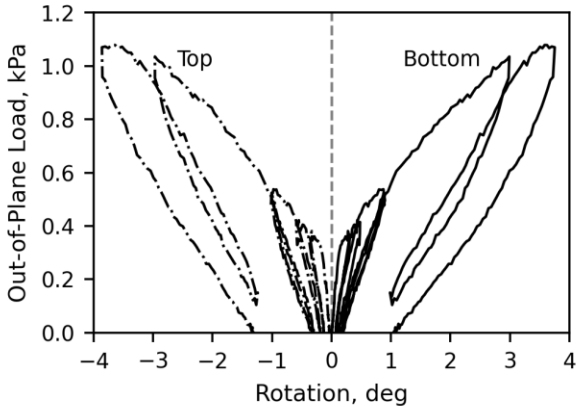

Figure 4.29: Rotation history on the wall supports.

Strain gauges were placed at several locations of the wall to provide information regarding the response of the materials to different levels of load and the behaviour of the cross-section during the test. Figure 4.30 shows the load-strain curves for concrete masonry units and steel bars in the indicated courses as an average of the right and left sides. The reason to have sensors on both sides

for each indicated course was to capture any differential readings that suggested torsional effects, as well as to have some data collection redundancy in case gauges failed or otherwise did not function.

In the case of concrete masonry units, strain gauges were installed on the surface of the compressive face of the wall. Values from all of these sensors were negative, indicating compressive strains. In Course 1 (closest to the bottom support) concrete strains remained close to zero during all cycles. In Course 39 (close to the top support) readings also were close to zero during all cycles. These values were expected for an ideal pin support at the top. Course 21 (closest to the effective mid-height of the wall) was expected to have the largest strains. However, the largest strains for concrete were recorded in Course 24. Courses 12, 18 and 21 had similar strain values, with maximum values close to 500 $\mu\varepsilon$ (negative). All compressive load-strains presented a linear response essentially. Strains in the concrete blocks did not get close to the estimated crushing value of 3000 $\mu\varepsilon$.

Steel bars were placed at the centre of the cross-section (95 mm from the compressive face). Tensile strains are shown as positive values. In Course 1, rebar strains did not change during the load-unload process at each cycle but increased between cycles (when out-of-plane loads were equal to zero). This may be explained by some effect of the whole structure settling during the time taken to prepare for every subsequent cycle. Strain gauge readings from Course 39 (right and left) and Course 24 (left) are not available due to sensor malfunction. Similar to the situation for concrete, maximum strains were recorded at Course 24. Steel reinforcement in Courses 24 and 21 exceeded the yield strain of 2200 $\mu\varepsilon$ seen in steel coupon tension tests. Lines at the yield strain are included in Figure 4.30 for reference. As mentioned before, yielding of the reinforcement close to the peak load of cycle 6 explained the plateau on the load-displacement curve and presented a risk for the stability of the wall. As per safety planning for these tests, loading was stopped soon after this point.

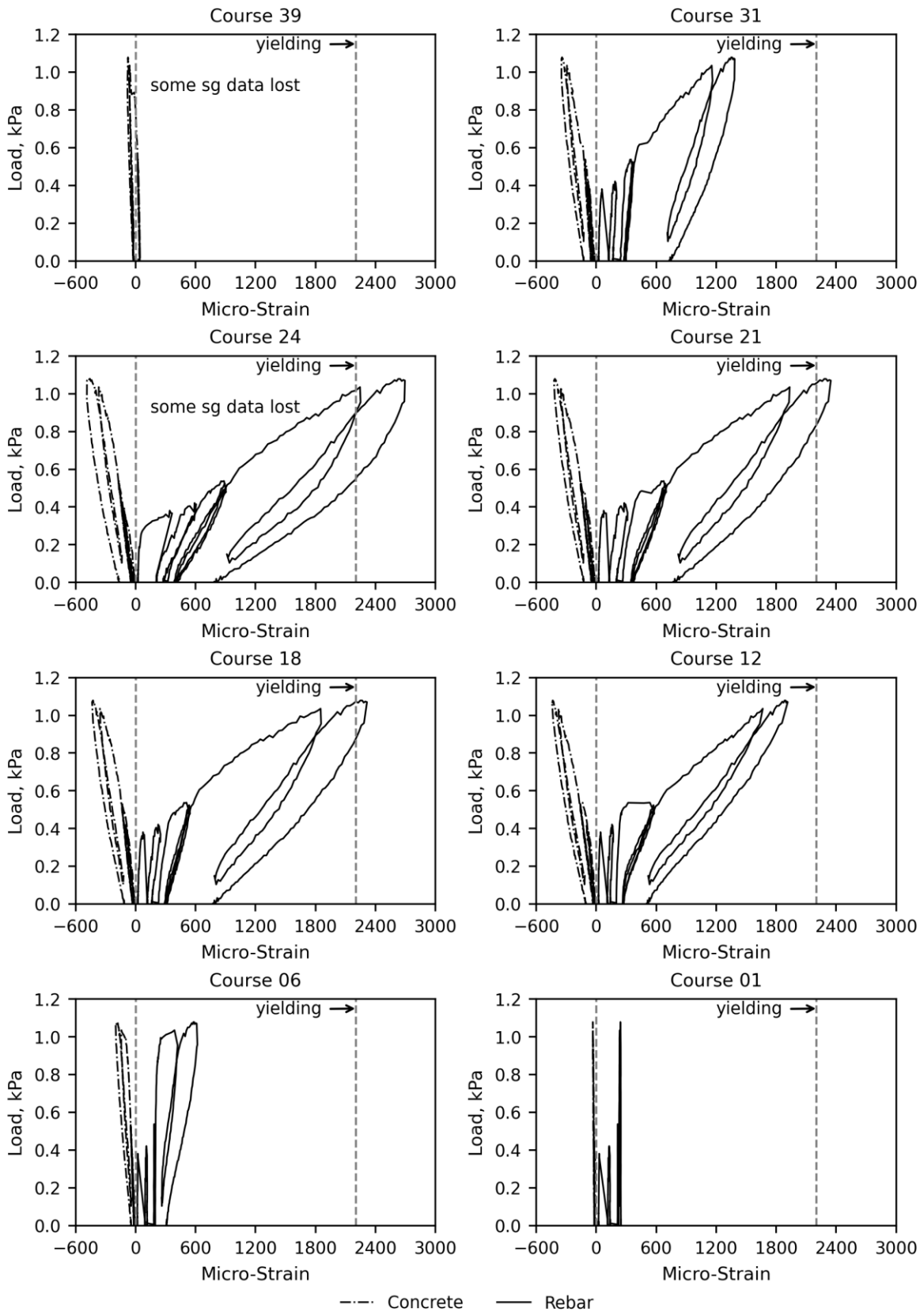

Figure 4.30: Strain history at several locations of the wall.

Magnitudes of midspan displacements, rotations, as well as compressive and tensile strains for every pinned-base cycle at peak load and after unloading are shown in Table 4.6.

Table 4.6: Midspan displacements and strains, and support rotations at peak load and after unloading for pinned-base cycles.

Cycle	Stage	Pressure, kPa	Midspan Displacement, mm	Bottom Rotation, deg	Top Rotation, deg	Strain on block at midspan, μm/m	Strain on rebar at midspan, μm/m
1	At peak load	0.37	18	0.3	-0.4	-94	100
	After unloading	-	-	-	-	-	-
2	At peak load	0.41	25	0.5	-0.6	-108	292
	After unloading	0.01	3	0.1	-0.2	-31	201
4	At peak load	0.50	48	0.9	-1.0	-155	694
	After unloading	0.01	8	0.2	-0.3	-41	348
5	At peak load	0.48	47	0.9	-1.0	-149	700
	After unloading	-0.03	8	0.2	-0.3	-42	357
6	At peak load	1.07	199	3.8	-3.9	-423	2347
	After unloading	0.00	55	1.1	-1.3	-124	771

As mentioned before, a water tank was filled with water until the two load cells at the top support had a reading of 15 kN total. The volume of water in the tank was constant for each cycle, so the same weight was hung from the top lever arm. Straps were tied from the tank to fixed points on the ground to keep the weight vertically aligned with the position of the lever arm. However, the tank moved slightly because of wind during the test.

It was important to record the magnitude of the vertical load to quantify second-order moments and understand their contribution to the total moment. Figure 4.31 shows the total load applied at the top of the wall over the entire test, varying between 14.1 and 15.2 kN. This may be attributed to some movement of the tank or to the misalignment of the load cells and the lever arm due to the rotation at the top support. The recorded loads were used to calculate second-order moments.

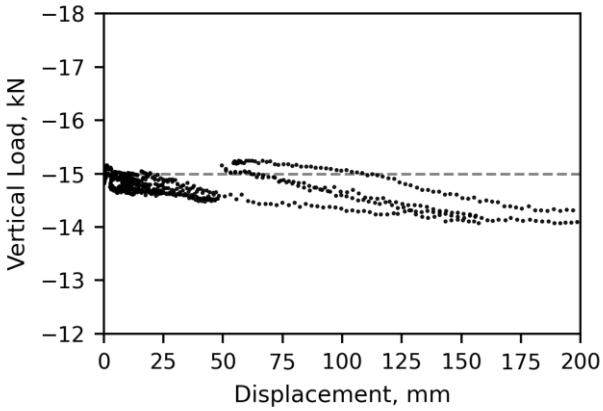

Figure 4.31: Total vertical load applied at the top of the wall during the test.

The distributed out-of-plane load applied on the surface of the wall, q, is estimated using Equation (4.1). This equation assumes that the recorded pressure from the airbag is applied uniformly on the surface that is in contact with the wall.

$$q = P_A \times b \tag{4.1}$$

Where P_A is the pressure measured in the airbag and b is the wall width.

First-order moments, M_{fo}, were calculated using Equation (4.2). First-order moments are composed of the moments induced by the eccentric vertical load at the top, present during the whole test, and the out-of-plane load applied by the airbag. Equation (4.2) is valid for a distributed load applied from the bottom to the top of the wall. This is untrue for this case since the airbag length (7.5 m) is shorter than the wall itself. The airbag was centrally positioned, leaving 625 mm of wall with no pressure at each end. However, comparing first-order moments from the idealized all-length load and the actual length of the airbag results in a maximum difference of 0.8% at midspan using numerical models. This suggests that results from Equation (4.2) are very close to reality.

$$M_{fo}(y) = q\left(\frac{y}{2}\right)\left(H_{eff} - y\right) + Pe\left(\frac{y}{H_{eff}}\right) \tag{4.2}$$

Where y is the height of the analyzed point on the wall from the pin base, H_{eff} is the effective height of the wall measured pin-to-pin (8835 mm), e is the eccentricity of the vertical load (170 mm), and P is the vertical load applied at the top of the wall (Figure 4.30).

Second-order moments are generated by the vertical load applied and the self-weight of the wall above the analyzed point multiplied by the displacement at that point. Second-order moments, M_{so}, are calculated using Equation (4.3).

$$M_{so}(y) = (P + P_{sw})\,\delta \tag{4.3}$$

Where P_{sw} is self-weight load and δ is the out-of-plan displacement at the point analyzed. Self-weight was obtained using Table B.1 from Drysdale and Hamid (2005) for a partially grouted wall with 190 mm hollow CMUs. Table B.1 assumes a concrete density of 2100 kg/m^3 and a grout density of 2350 kg/m^3, resulting in a wall self-weight of 2.19 kN/m^2 for ungrouted walls and 4.12 kN/m^2 for grouted walls. For partially grouted, self-weight may be calculated based on linear interpolation. For two grouted cells out of six, the wall would be expected to weigh $(2(4.12) + 4(2.19))/6 = 2.83$ kN/m^2. Using these numbers P_{sw} results in approximately 14.8 kN at the wall midspan, which is essentially the same as the vertical load P (15 kN). This suggests that for slender walls with low axial loads, self-weight is a major influence on second-order moments.

The total moment, M_{total}, on the wall was obtained by adding the first-order moments from Equation (4.2) and the second-order moments from Equation (4.3), as shown in Equation (4.4).

$$M_{total} = M_{fo} + M_{so} \tag{4.4}$$

Figure 4.31 presents midspan moment-displacement curves, showing first-order and second-order moments as well as the total moment during the test. The reason to show information from midspan is that the maximum moments were expected at this point due to the boundary conditions of the structure. Second-order moments are seen as a straight line since they increase linearly with displacement. The wall stiffness decreased after cracking; therefore, it deflects considerably more as the load is increased beyond cracking, and second-order moments have an increasingly larger influence on the response of the wall. At the end of cycle 6, vertical reinforcement started to yield (Figure 4.30). This is also shown in the way that the first-order moment curve plateaus close to the maximum displacement of 200 mm. However, the total moment keeps increasing due to the growing second-order moment.

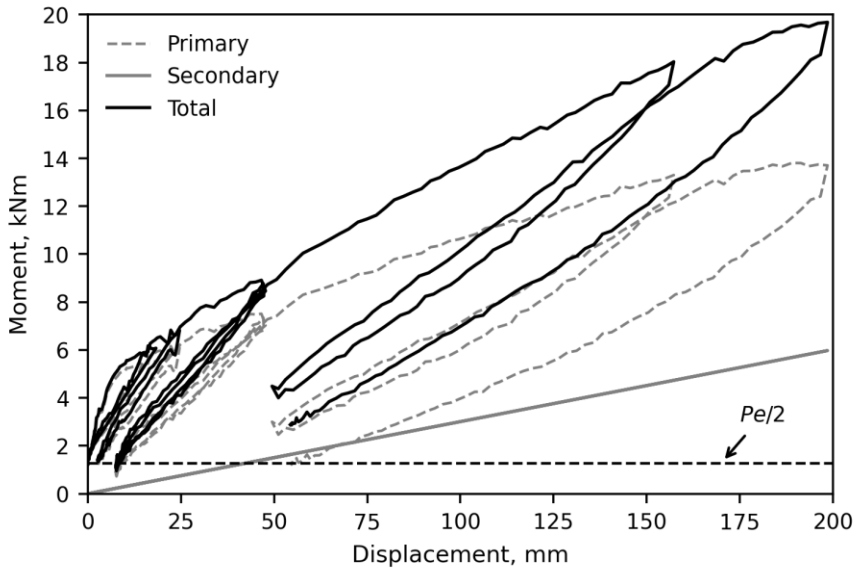

Figure 4.32: Midspan moment-displacement curve.

Using Equations 4.1 to 4.4, we can calculate moments at each point where displacements are known. Using information from string potentiometers installed on the wall, Figure 4.33 presents the maximum total moment profile of the wall for each cycle. It draws a parabolic shape as expected, with a constant moment of Pe at the top support that reduces to zero at the bottom support. To visualize the composition of the total moment on the wall at a given time, Figure 4.34 shows the different contributions of first and second-order moments to the complete moment profile. First-order moments are decomposed into moments from the eccentric vertical load (Pe moment) and those from the out-of-plane load (OOP moment) for convenience.

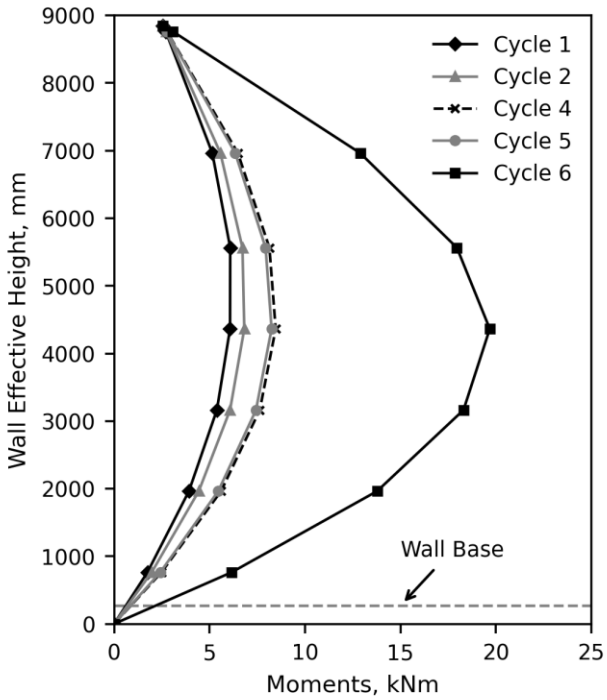

Figure 4.33: Total moment profiles for the pinned-base cycles.

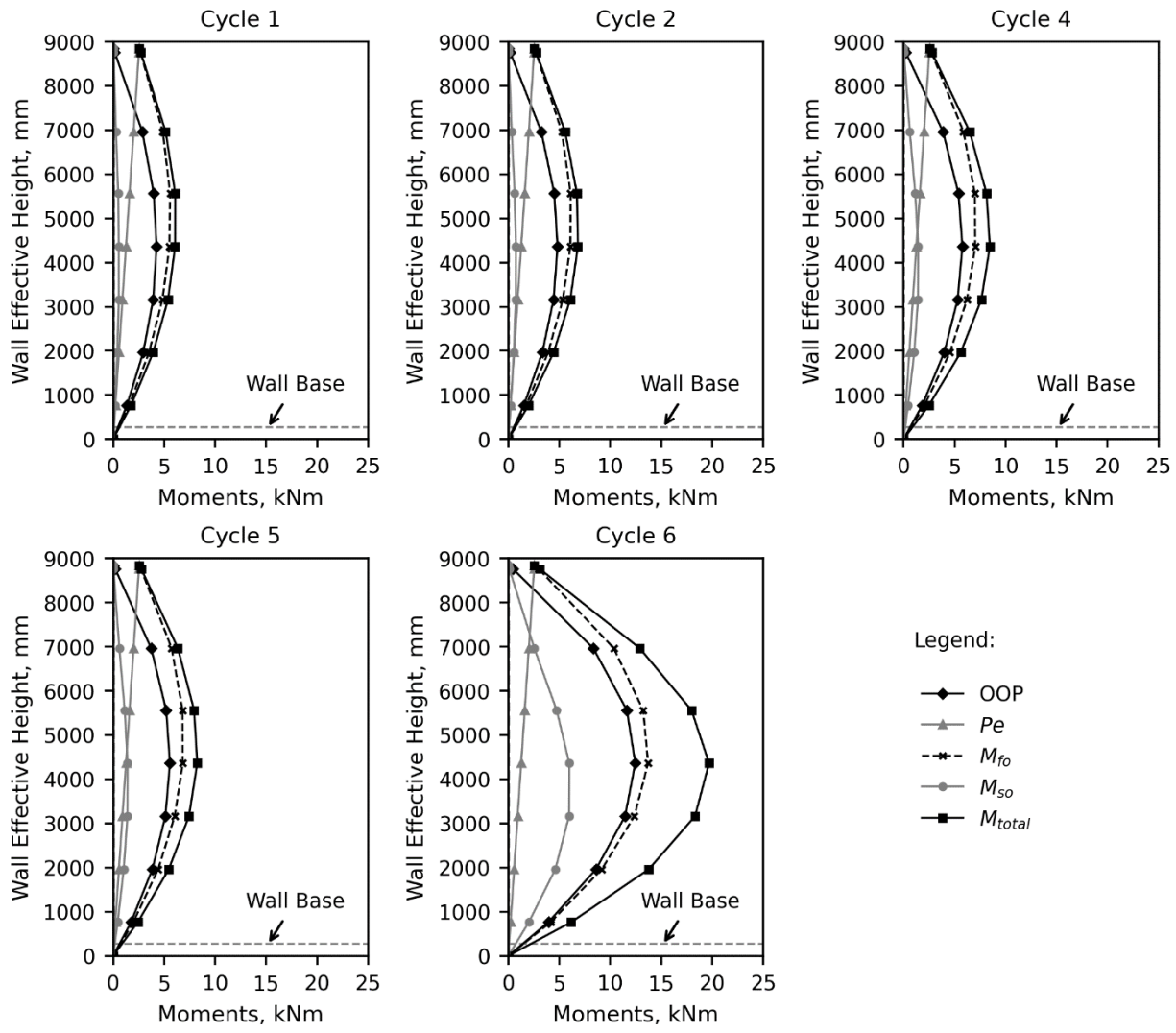

Figure 4.34: Moment composition profiles for pinned-base cycles.

Since the vertical load *P* is essentially constant aside from small variations previously discussed (Figure 4.31), *Pe* moment is the same for all graphs (~2.55 kNm). OOP moment comprised much of the first-order moment for all cycles: 74%, 76%, 80, 79% and 90% of the first-order moment at midspan at peak load for cycles 1, 2, 4, 5 and 6, respectively. In cycles 1 to 5, second-order moments were relatively small; for instance, 1.40 kNm at midspan at peak load in cycle 5 and 19% of the overall total moment. Cycle 6 is where second-order moments became a considerably larger factor, being 5.95 kNm and 33% of the total midspan moment. As discussed before, the vertical bars started yielding close to the peak load in cycle 6. It can be assumed that if the wall were

pushed further, it would have experienced very large displacements while second-order moments continued to increase with a risk of stability failure (buckling).

The strain profile of the section can be drawn at every course where strain gauges were installed. Drawing strain profiles from different parts of the test can help visualize strain development in the section. Figure 4.35 shows the strain profiles at peaks loads for every cycle. Again, strain values for concrete are the average of the recorded strains on right and left sides; the same applies to strains on rebar. A straight line is drawn from the strain in concrete to the strain of rebar, representing the linear relationship between these points due to the assumption that plane sections remain plane in a flexural governed structure. The location where this line intercepts the *x*-axis is defined as the neutral axis, and it is where strains change from being compressive (negative) to being tensile (positive). Vertical bars are assumed to be centrally located in the cross-section at 95 mm from the compressive face of the wall; however, steel bars could have moved from this location during the construction process and especially when pouring grout into the cells.

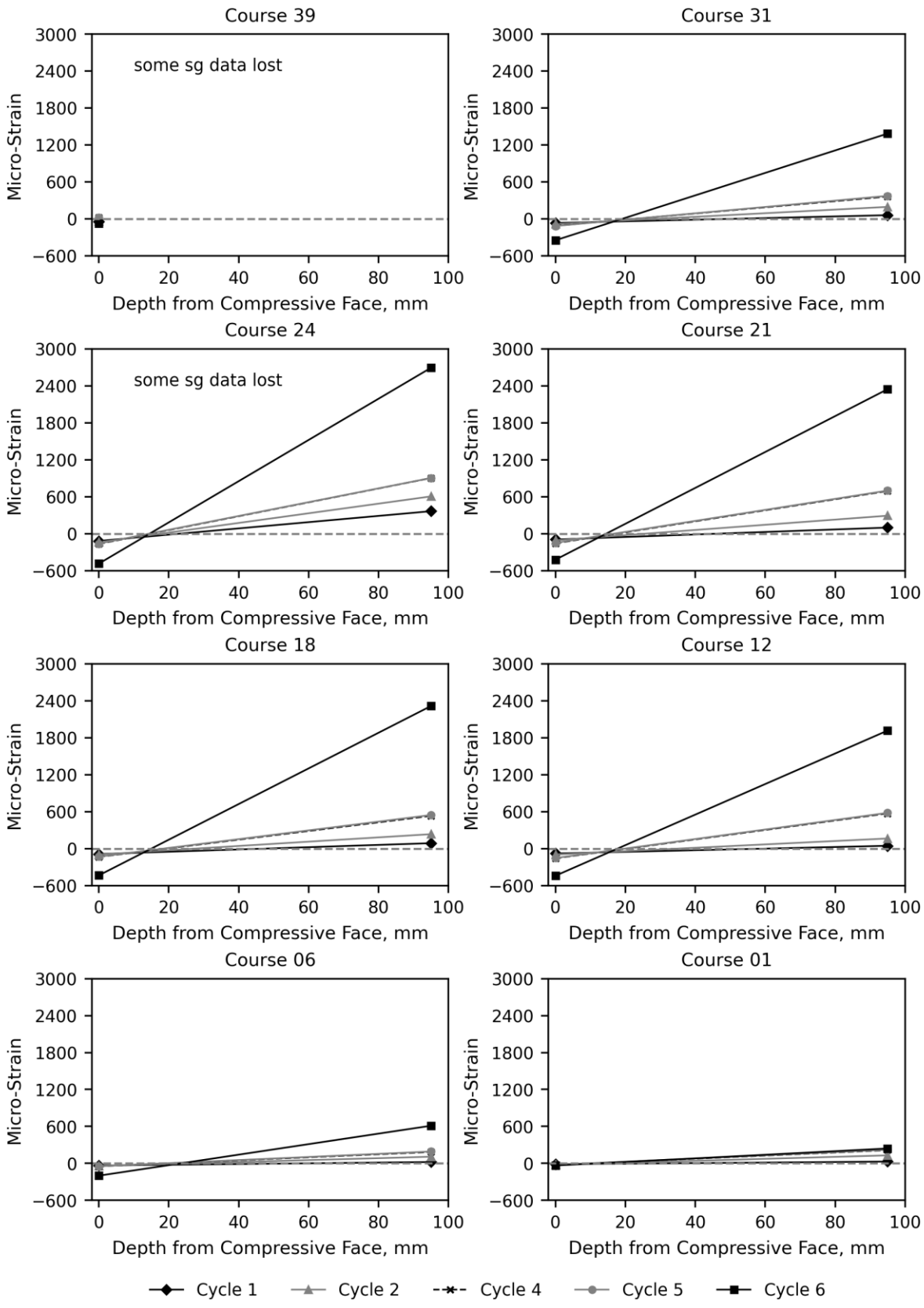

Figure 4.35: Strain profiles at several courses of the wall at peak load of each cycle.

Course 39 does not have strain profiles due to the lost rebar strain gauges. In courses close to the supports (Courses 1, 6 and 31) strains were relatively low, particularly for cycles 1 to 5. The profiles are almost horizontal, meaning very small curvature due to the small moments present in those courses. Courses closer to the centre of the wall (Courses 12, 18, 21, 24) show much more obvious slopes of the lines from cycles 1 to 6. Despite the differences, all courses showed that the neutral axis was within the face shell of the concrete block from the early stages of loading. This means that the grouted portion of the cross-section contributed very little to the wall response, probably only before cracking. Still, it is important to note that grout remains essential for this wall configuration as it keeps embedded steel bars in position and makes it possible for the interaction between bars and masonry to work as one element.

Magnitudes of out-of-plane and vertical load, midspan moments and curvature for every pinned-base cycle at peak load and after unloading are presented in Table 4.7.

Table 4.7: Loads, moments and curvature at peak load and after unloading for pinned-base cycles.

Cycle	Stage	Vertical Load, kN	Pressure, kPa	1st order Moment, kN-m*	2nd order Moment, kN-m*	Total Moment, kN-m*	Curvature, 1/km*
1	At peak load	-15.0	0.37	4.83	0.55	5.38	1.6
	After unloading	-	-	-	-	-	-
2	At peak load	-14.8	0.41	5.34	0.73	6.07	3.4
	After unloading	-14.7	0.01	0.99	0.08	1.07	2.0
4	At peak load	-14.5	0.50	6.22	1.42	7.63	7.2
	After unloading	-14.8	0.01	1.03	0.23	1.26	3.3
5	At peak load	-14.5	0.48	6.03	1.40	7.43	7.2
	After unloading	-14.9	-0.03	0.56	0.23	0.79	3.4
6	At peak load	-14.1	1.07	12.35	5.95	18.31	23.5
	After unloading	-15.2	0.00	0.96	1.59	2.56	7.6

* at midspan

4.7.2 Results vs Expected Response

The numerical model presented in Chapter 3 defines a wall subject to a constant eccentric vertical load and a monotonic out-of-plane load. Readings from the test and the curve from the model are presented together in Figure 4.36.

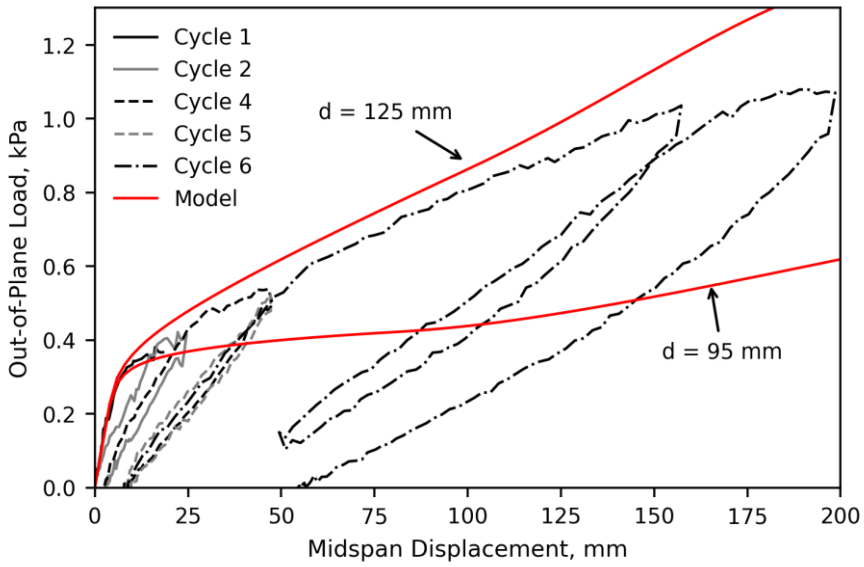

Figure 4.36: Load displacement comparison, test results and numerical model prediction.

During the first cycle up to around 0.3 kPa the wall response was linear, and the line from the numerical model response overlapped with the loading points from the test. It can be assumed that no major cracking occurred during this stage, and masonry properties govern the response. From 0.3 kPa and 0.5 kPa of out-of-plane load the stiffness of the wall greatly reduced, as it was at this stage when most of the cracks at the joints were developed. The behaviour of the wall after cracking, extending from 0.3 kPa to the peak load at the end of the test, was mainly affected by the vertical reinforcement in the cross-section. It is observed in the graph that defining $d = 95$ mm (corresponding to the assumption that vertical steel bars were at the exact centre of the cross-section) results in underestimation of the wall stiffness. The model predicts an applied load of 0.62 kPa for the maximum displacement of 200 mm, merely 58% of the pressure recorded during the test at the same displacement.

As discussed in the parametric analysis from chapter 3, a small variation of steel area or bar depth greatly affects the response of slender walls, as they change the post-cracking stiffness of the wall and the resulting stresses on the rebar. Therefore, vertical steel bars may have deviated from their original position farther from the compressive face of the wall during the grouting process, resulting in a larger post-cracking stiffness and a larger yielding load. Using $d = 125$ mm to estimate the wall response with the numerical model results in a curve that fits better with the actual response of the wall, yet a better value could be assumed if needed. At about 1.0 kPa of out-

of-plane pressure, the wall reinforcement yielded during the test; it can be observed that load was almost constant while the displacement kept increasing at this stage. However, the model response did not present yielding in this range of loads for any of both proposed values of d.

Curvature is the rate of change for strains in the cross-section, as shown in Figure 4.37. It was possible to get the measured curvature, ψ, by knowing the strains in the cross-section and applying Equation (4.5).

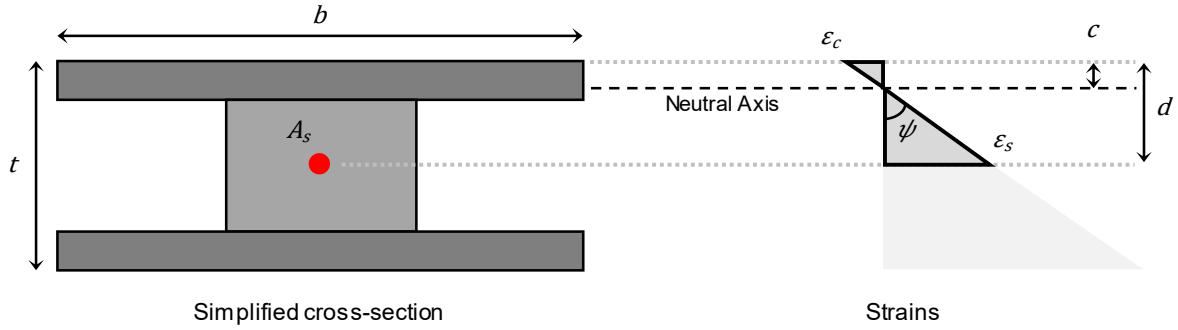

Figure 4.37: Schematic of the strains and curvature in the wall cross-section.

$$\psi = \frac{\varepsilon_s - \varepsilon_c}{d} \tag{4.5}$$

Where ε_c is the strain in concrete, ε_s is the strain in rebar, and d is the depth of the vertical reinforcement measured from the compressive face of the wall. Both considered values of d, 95 mm and 125 mm, were used in Figure 4.38 to compare the moment-curvature of the wall cross-section during the test against the values predicted with the numerical model. Even though $d = 125$ mm results in a closer response of the model to that of the tested wall according to the load-displacement curve, the model curve in the moment-curvature diagram did not get as close to the test curve. Moment magnitudes from the test are the same for both cases since the moment is calculated according to the known geometry of the wall and the loading conditions. Only curvature is affected by the change of reinforcement depth. This suggests that different loading conditions may have been present in the test, such as a differential pressure applied by the airbag. The actual depth of the steel bars will be obtained by a future forensic inspection of the masonry wall after demolition; this will help clarify how much this deviation, if any, was affecting the wall response of the wall. So far, there is not enough data to get a conclusive statement on this effect.

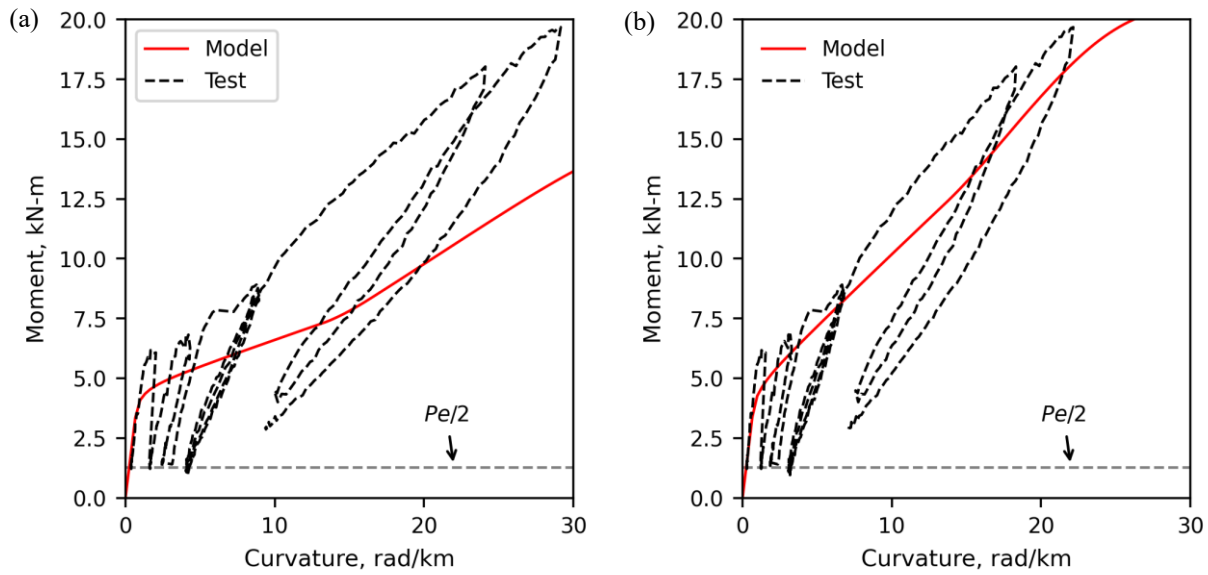

Figure 4.38: Moment-curvature comparison of test results and numerical model prediction. (a) Bars assumed to be centrally located at *d* = 95 mm (b) Bars assumed to be deviated at *d* = 125 mm.

4.8 Fixed-Base Cycle

A comparison of the response of the wall in the uncracked-elastic range was performed using cycles 2 (pinned-base) and 3 (fixed-base) results. Figure 4.39 shows the load-displacement curve for both base conditions. From an out-of-plane load of 0 to 0.10 kPa, the slopes are very similar for both cycles. However, after 0.10 kPa, the curves deviate from each other. For instance, at an out-of-plane load (0.35 kPa), the midspan displacement for the pinned base wall was 1.75 times that of the fixed base wall. Displacement profiles of the wall at a load of 0.35 kPa for cycles 2 (pinned-base) and 3 (fixed-base) are shown in Figure 4.40a. At a midspan displacement of 8.34 mm, the peak displacement for the fixed-base cycle, the out-of-plane load for the fixed-base condition was 1.66 times the load required for the pinned-base condition. Displacement profiles for a midspan displacement of 8.34 mm are compared in Figure 4.40b.

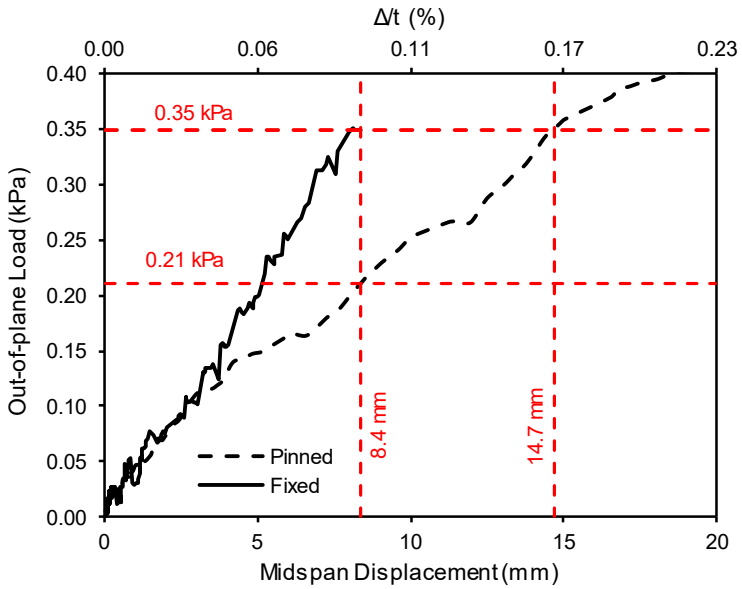

Figure 4.39: Load-displacement history, comparing pinned and fixed base conditions.

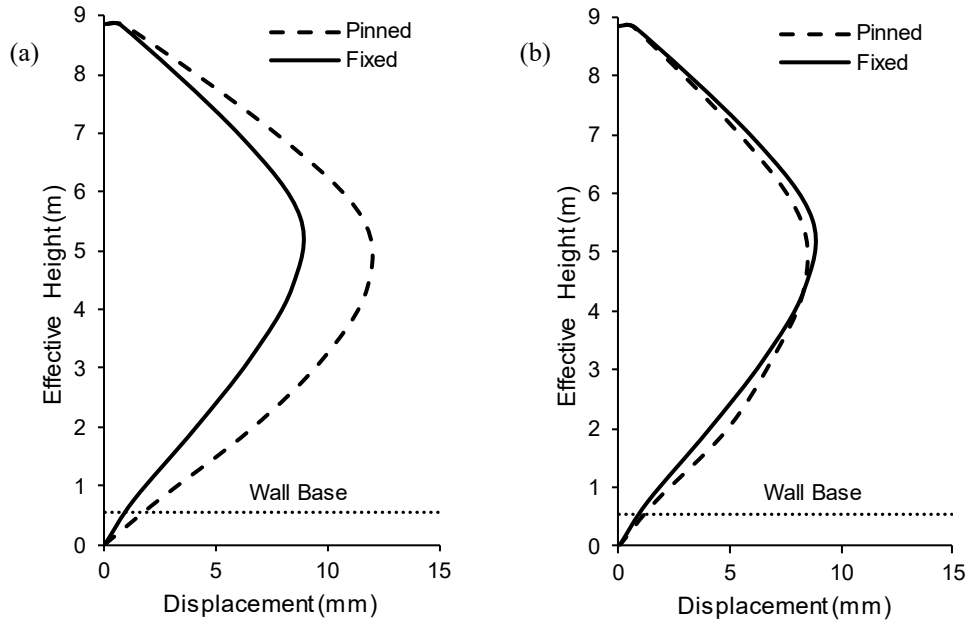

Figure 4.40: Displacement profile comparison: (a) Same out-of-plane load - 0.35 kPa (b) Same midspan displacement - 8.4 mm

Slender masonry walls are traditionally believed to develop a plastic hinge at the base relatively early during cyclic loading due to a degradation of the connection between the wall and its foundation. Therefore, CSA S304 requires walls with an *h*/*t* ratio of more than 30 to be analyzed under pinned-pinned conditions regardless of actual boundary conditions. The comparison offered in this section shows that there is a beneficial effect of a rigid base at service conditions for reducing out-of-plane displacements. A limitation of this comparison is that the response of the

wall under both base conditions was compared under small loads, and any investigation about the base degradation applying cyclic out-of-plane load was out of the scope of this study.

5 SUMMARY AND CONCLUSIONS

5.1 Summary

Single-storey slender masonry walls are commonly used in structures such as school gymnasiums and light industrial buildings. North American standards (CSA S304-14, TMS 402-16) require walls with a height-to-thickness ratio of 30 or higher to satisfy several stringent requirements like assuming a pinned support at the base and limiting the compressive axial load. The reason for these restrictions is that slender walls are more sensitive to second-order effects due to the large out-of-plane displacements they experience during loading, and it is believed that they present early instability issues. There is no evidence to prove this right, and recent studies show that design standards are overly conservative, leading to non-economical designs. Therefore, further testing is needed to provide results for the proposal of less conservative design criteria.

This study was the start of an experimental research campaign at the University of Alberta with three main objectives: characterize the response of slender concrete-masonry walls under a combination of axial and out-of-plane loads, assess the performance of the current Canadian masonry design standard for slender masonry walls and generate a rational and modern design procedure. Chapter 2 presented a literature review to understand the techniques available to analyze the response of slender masonry walls and the research efforts to get rational design criteria for such walls during the last 50 years. Chapter 3 presented a computer-based numerical model developed to predict the behaviour of slender masonry walls under axial and out-of-plane loads. Validation of the model was conducted based on previous experimental studies. Chapter 4 detailed the design of an innovative test setup capable of testing 8.75 m wall specimens under a combination of axial and out-of-plane loads. This design was partially based on the ACI-SEAOSC field tests performed in 1980. Chapter 4 also presented a test of an 8.75 m wall with a height-to-thickness ratio of 46 and pin-pin supports, subject to a sustained eccentric vertical load, representing the gravity loads coming from the roof system, and an increasing out-of-plane load, representing wind pressure or seismic forces applied to the wall. Discussion of test results was included.

5.2 Conclusions

Conclusions drawn from the analytical and experimental phases of this study on slender masonry walls are as follows.

From Chapter 3, where a numerical model to investigate the second-order response of SMW with various reinforcement layouts:

- The proposed numerical model closely predicts the out-of-plane response of SMWs subject to low axial loads and under various conditions. A limitation of the model is that it does not predict any local effects like the crushing of the masonry near the supports, spalling of concrete from the face shells or reduced bonding of the reinforcement. This is due to the macro-modelling nature of the model.
- Chapter 3 presented a section where the steel rebar is touching the inner face of the CMU in an effort to increase the moment arm and reduce second-order effects (Wall 3). This appears to be a promising solution according to model predictions.
- Results of the parametric study in Chapter 3 showed that slender walls encounter instability at or shortly after the reinforcement yields, suggesting that ductility does not play a significant role in the response.

From Chapter 4, where a test setup was presented along with results from a SMW built with details common in construction practice, the following was concluded:

- The test setup worked as intended. The SMW had a response expected for the loading and support conditions of the test. The load-displacement curve showed an essentially linear pre-cracked stiffness, followed by the development of cracks, then an essentially linear post-cracked stiffness and eventually a plateau that indicates yielding of rebar. All displacement profiles had a single curvature with a parabolic shape and the largest displacement at midspan. Rotations measured at both top and bottom supports were virtually the same.
- The importance of needing a displacement limit in the standards was evident. Cycles 4 and 5 pushed the wall to a midspan displacement equal to the serviceability limit of $h/180$

required by S304-14 (48 mm). After unloading, the residual displacement at midspan was already equal to 8 mm, indicating damage and loss of out-of-plane stiffness.

- After plotting strain profiles for the courses where strain gauges were located, it was found that the neutral axis was within the face shell of the concrete block from the early stages of loading. This means that the grouted portion of the cross-section contributed very little to the wall response, likely only before cracking. It also shows the importance of having the ungrouted properties of the masonry well defined, as they seem to govern most of the response of these walls.
- Slender masonry walls are traditionally believed to develop a plastic hinge at the base relatively early during cyclic loading due to a degradation of the connection between the wall and its foundation. A comparison offered in section 4.8 shows a beneficial effect of a rigid base at service conditions for reducing out-of-plane displacements. For instance, at an out-of-plane load (0.35 kPa), the midspan displacement for the pinned base wall was 1.75 times that of the fixed base wall. No signs of degradation of the base were observed. A limitation of this comparison is that it was performed under small loads, and only one loading cycle was performed under a pinned-base condition.

After comparing test results against numerical model estimations, the following conclusions were drawn:

- The behaviour of the wall after cracking was mainly dictated by the vertical reinforcement. When defining d = 95 mm in the numerical model (assuming that vertical bars were at the centre of the cross-section), wall stiffness is underestimated. This may be explained if steel bars moved from the original position during construction. Any deviation greatly affects the response of slender walls, changing the post-cracking stiffness and the resulting stresses on the rebar, as discussed in Chapter 3. Therefore, vertical steel bars may have deviated from their original position farther from the compressive face of the wall during the grouting process, resulting in a larger post-cracking stiffness and a larger yielding load. Defining d = 125 mm results in a curve that fits better with the actual response of the wall.
- Even after matching the model load-displacement estimation with test results, the moment-curvature at midspan did not match. Additionally, strain gauges reported the largest strains

three courses above midspan, suggesting that the maximum moment may not be located at midspan. It is concluded that a different nature of the loading conditions may have been present during the test, such as a differential pressure applied by the airbag or some friction present at the supports.

Due to time constraints and lab access, masonry prisms could not be tested at the time of writing. Also, a forensic inspection of the wall tested was planned in the near future to assess the position of steel bars during construction. Both will provide valuable information to calibrate the numerical model further and reveal how the test may have deviated from idealized loading conditions.

5.3 Recommendations for future work

This thesis aimed to serve as a starting point for a research campaign to test slender masonry walls under different configurations. An innovative test setup was designed, and a full-scale slender masonry wall, conventionally designed and built, was tested. The setup will continue to be used for future tests, and results from this test will be used as a reference to compare with other wall configurations. There are a series of recommendations for future work based on the outcomes of this study:

1. A more in-depth study must be conducted on the ductility requirements found in S304-14 for slender walls. Future studies should explore the failure modes of a wider range of slender masonry walls.
2. A few problems were encountered with the test setup, such as the airbag making contact with some string potentiometers and the pressure gauge being affected by the airflow from the compressor. Correcting these issues will make it easier to perform tests and analyze data.
3. A comparison between pinned-base and fixed-base conditions was included in this study. A limitation of this comparison is that the wall was subject to very small out-of-plane loads (~0.35 kPa), and an investigation about the base degradation applying cyclic out-of-plane load was out of the scope of this study. Future studies should include variations on the base condition and cyclic out-of-plane loads to evaluate any degradation at the base.
4. In slender masonry walls, second-order effects become especially relevant for large axial loads. Therefore, future tests should explore the effects of the axial load when successively

increased and may explore the loading condition for which the failure mechanism changes from strength to stability.

5. Future tests on slender masonry walls should include variations on the vertical reinforcement ratio and the position of bars to investigate how these changes affect the response and failure mode on these walls.
6. In this study, an 8.75 m masonry wall was subject to a constant axial load and an increasing out-of-plane load until signs of yielding of the reinforcement were observed. The wall was not pushed to failure due to safety concerns. However, adapting the test setup may allow to push the wall to failure to evaluate ductility and effective stiffness in slender walls.
7. Once that more data is available, like the compressive strength of the masonry prisms and the forensic inspection of the location of the steel bars, the calibration of the model can be completed. At that point, it should be evaluated if the model proposed is adequate to evaluate the response of slender masonry walls or a more refined micro-model will be needed.
8. Future wall tests should be complemented with a parametric study using the numerical model, including different heights, base fixities, loading conditions, and reinforcement configurations. All this data will help to propose rational and modern design criteria for slender masonry walls.

REFERENCES

Abboud, B. E., Hamid, A. A., and Harris, H. G. (1996). "Flexural behavior of reinforced concrete masonry walls under out-of-plane monotonic loads." *ACI Structural Journal*, 93(3), 327–335.

ACI-SEASC Task Committee on Slender Walls. (1982). *Test Report on Slender Walls*. Los Angeles, United States.

Alonso, A., Gonzalez, R., Cruz, C., and Tomlinson, D. (2021). "Pre-Test Analysis of the Effect of Rotational Base Stiffness on Loadbearing Slender Masonry Walls." *14th Canadian Masonry Symposium*, Montreal, Canada.

ASTM A01 Committee. (2020). *Specification for Deformed and Plain Carbon-Steel Bars for Concrete Reinforcement*. ASTM International.

Bean Popehn, J. R., Schultz, A. E., and Drake, C. R. (2007). "Behavior of Slender, Posttensioned Masonry Walls under Transverse Loading." *Journal of Structural Engineering*, 133(11), 1541–1550.

Bilotta Rios, M., and Cruz Noguez, C. (2021). "Evaluation of Second-Order Effects in Slender Reinforced Masonry Walls." *14th Canadian Masonry Symposium*, Montreal, Canada.

Canadian Standards Association. (2014). *CSA A179-14 Mortar and Grout for Unit Masonry*.

Canadian Standards Association. (2014). *CSA A371-14 Masonry Construction for Buildings*. Toronto, Canada.

Canadian Standards Association. (2014). *S304-14 Design of Masonry Structures*. Mississauga, Canada.

Canadian Standards Association. (2014). *A-165 Series-14: CSA Standards on Concrete Masonry Units*. Toronto, Canada.

Da Porto, F., Mosele, F., and Modena, C. (2011). "Cyclic Out-of-Plane Behaviour of Tall Reinforced Masonry Walls under P–Δ Effects." *Engineering Structures*, 33(2), 287–297.

De Lorenzis, L., and Teng, J. G. (2007). "Near-surface mounted FRP reinforcement: An emerging technique for strengthening structures." *Composites Part B Engineering*, 38(2), 119–143.

Donà, M., Tecchio, G., and Da Porto, F. (2018). "Verification of second-order effects in slender reinforced masonry walls." *Materials and Structures*, 51(3), 51–69.

Drysdale, R. G., and Hamid, A. A. (2005). *Masonry structures: Behaviour and design (Canadian edition)*. Canada Masonry Design Centre, Mississauga, Canada.

Entz, J. (2018). "Development of Innovative in-Line Stiffening Element for Out-of-Plane Masonry Walls." Master's Thesis, University of Alberta.

Entz, J., Cruz Noguez, C., Guzman Sanchez, O., and Banting, B. (2017). "Tall Masonry Walls with In-Line Boundary Elements." *13th Canadian Masonry Symposium*, Halifax, Canada.

European Committee for Standarization. (2005). *Eurocode 6 - Design of Masonry Structures - Part 1-1: General rules for Reinforced and Unreinforced Masonry Structures*. Brusseles, Belgium.

Gonzalez, R., Alonso, A., Cruz, C., and Tomlinson, D. (2021). "Numerical Study of the Response of Reinforced Slender Masonry Walls with various Reinforcement Arrangements." *14th Canadian Masonry Symposium*, Montreal, Canada.

Hamid, A. A., Abboud, B. E., Farah, M. W., Hatem, M. K., and Harris, H. G. (1989). *Response of Reinforced Block Masonry Walls to Out-of-Plane Static Loads*. Drexel University, Philadelphia, Pennsylvania.

Hatzinikolas, M., Longworth, J., and Warwaruk, J. (1978). *Structural Engineering Report 70, Concrete Masonry Walls*. University of Alberta, Edmonton, Canada.

Il Ministro Delle Infrastrutture. (2008). *Decreto del Ministero delle infrastrutture DM-14-01-2008*. Roma, Italia.

Isfeld, A. C., Müller, A. L., Hagel, M., and Shrive, N. G. (2019). "Analysis of safety of slender concrete masonry walls in relation to CSA S304-14." *Canadian Journal of Civil Engineering*, 46(5), 424–438.

Isfeld, A. C., Müller, A. L., Hagel, M., and Shrive, N. G. (2021). "Testing and finite element modelling of concrete block masonry walls under axial and out-of-plane loading." *International Journal of Masonry Research and Innovation*, 6(1), 60–80.

Korany, Y., and Drysdale, R. (2006). “Rehabilitation of Masonry Walls Using Unobtrusive FRP Techniques for Enhanced Out-of-Plane Seismic Resistance.” *Journal of Composites for Construction*, 10(3), 213–222.

Lirola, J. M., E. Castañeda, B. Lauret, and M. Khayet. (2017). “A review on experimental research using scale models for buildings: Application and methodologies.” *Energy Build.*, 142: 72–110.

Liu, Y., and Dawe, J. L. (2001). “Experimental determination of masonry beam-column behaviour.” *Canadian Journal of Civil Engineering*, 28(5), 794–803.

Liu, Y., and Hu, K. (2007). “Experimental Study of Reinforced Masonry Walls subjected to Combined Axial Load and Out-of-Plane Bending.” *Canadian Journal of Civil Engineering*, 34(11), 1486–1494.

Mac Gregor, J. G., Bree, J. E., and Pfrang, E. O. (1970). “Design of slender concrete columns.” *ACI Journal*, 67(2), 6–28.

Masonry Standards Joint Committee. (2002). *Specification for Masonry Structures (ACI 530.1-02/ASCE 6-02/TMS 602-02)*.

McKenna, F., Scott, M. H., and Fenves, G. L. (2010). “Nonlinear Finite-Element Analysis Software Architecture Using Object Composition.” *Journal of Computing in Civil Engineering*, 24(1), 95–107.

Mohammed, A., T. G. Hughes, and A. Mustapha. (2011). “The effect of scale on the structural behaviour of masonry under compression.” *Construction and Building Materials*, 25 (1): 303–307.

Mohsin, E., and Elwi, A. E. (2003). “Effect of Implied Fixity at Masonry Block Wall-Support interface on Stability of Load Bearing Walls.” *Annual Conference of the Canadian Society for Civil Engineering*, Nouveau-Brunswick, Canada.

Müller, A. L., Isfeld, A. C., Hagel, M., and Shrive, N. G. (2017). “Review and Analysis of Capacity of Slender Concrete Masonry Walls.” *13th Canadian Masonry Symposium*, Halifax, Canada.

Parvin, A., and Syed Shah, T. (2016). “Fiber Reinforced Polymer Strengthening of Structures by Near-Surface Mounting Method.” *Polymers*, 8(8), 298.

Petit, C. E. J. (2019). “Effect of Rotational Base Stiffness on the Behaviour of Loadbearing Masonry Walls.” Master’s Thesis, University of Alberta.

Pettit, C., and Cruz-Noguez, C. (2021). “Effect of Rotational Base Stiffness on the Behavior of Load-Bearing Masonry Walls.” *Journal of Structural Engineering*, 147(12), 04021215.

Robazza, B. R., Brzev, S., Yang, T. Y., Elwood, K. J., Anderson, D. L., and B., M. (2018). “Out-of-Plane Behavior of Slender Reinforced Masonry Shear Walls under In-Plane Loading Experimental Investigation.” *Journal of Structural Engineering*, 144(3), 04018008.

Sparling, A., and Palermo, D. (2021). “Out-of-Plane Cyclic Response of Slender Reinforced Masonry Walls Subjected to Increasing Axial Load.” *14th Canadian Masonry Symposium*, Montreal, Canada.

Sparling, A., Palermo, D., and Hashemian, F. (2018). “Out-of-Plane Flexural Response of Hollow Masonry Walls with Near-Surface Mounted Reinforcement.” *10th International Masonry Conference*, Milan, Italy.

Sparling, A., Palermo, D., and Hashemian, F. (2021). “Out-of-Plane Flexural Testing and Stiffness Response of Concrete Masonry Walls with NSM Steel Reinforcement.” *Canadian Journal of Civil Engineering*, 48(7), 749–762.

The Masonry Society. (2016). *TMS 402/602-16 Building Code Requirements and Specification for Masonry Structures*. Longmont, U.S.

Xu, H. (2018). *Helical Pile Set-Up Time Effect and Helical Pile Torque-to-Capacity Correlation*. University of Alberta, Edmonton, Alberta.

Yokel, F. Y., Mathey, R. G., and Dikkers, R. D. (1970). *Compressive Strength of Slender Concrete Masonry Walls*. U.S. National Bureau of Standards, Washington, U.S.

Yokel, F. Y., Mathey, R. G., and Dikkers, R. D. (1971). *Strength of Masonry Walls Under Compressive and Transverse Loads*. U.S. National Bureau of Standards, Washington, U.S.